공학박사학위논문

A STUDY ON THE HOT CRACKING BEHAVIOR OF LASER WELDED ALUMINUM ALLOY FOR AUTOMOTIVE INDUSTRY

알루미늄 레이저용접부의 고온균열 거동에 대한 연구

2018년 **8**월

서울대학교 대학원

재료공학부

강 민 정

ABSTRACT

The laser was first introduced into the microelectronics industry in the late 1960s for sealing electronic packages and thin-wire connections. At present, laser welding is a proven joining technique in the automotive, metals (parts supply), shipyard, microelectronics, packaging, and aerospace industries. A laser has a high-power density heat source. Therefore, 'laser welding' is recognized as an advanced process to join materials with a laser beam of high-power, high-energy density. Laser welding promising joining technology with high quality, high precision, high performance, high speed, good flexibility and low distortion. Consequently, application of laser welding is increasing with the development of novel laser apparatuses and joining processes.

On the other hand, the development and commercialization of electric cars and hybrid cars, the application of aluminum to car body is gradually expanding. However, solidification cracking is frequently observed in aluminum welds. The low ductility of a semi-solid in the mushy zone and the high solidification shrinkage of aluminum alloys both increase hot cracking susceptibility. Solidification cracking is initiated by complex interactions between metallurgical and mechanical factors not by one factor. During laser welding, this can be diminished by improving chemical composition, refining

solidification structure, optimizing laser pulsing parameters, and/or reducing thermal strains. This is very important that deep understanding for the affecting factors to suppress the hot cracking propagation during laser welding, Since the changing of chemical composition by adding a filler wire is not practical for the laser welding, the effects of thermal cycle and residual stress of the welds have to be considered more seriously.

Various laser welding process was selected to change the thermal cycle. Also, these effects on microstructural and mechanical properties were investigated, too. Therefore, the complex physics during laser welding depending on penetration depth, the finite element method based on the thermal conduction was conducted for the simulation.

Microstructural evolution highly related with thermal cycle resulted from temperature gradient and solidification rate. According to the welding parameters, the width of equiaxed region was varied and the direction of grain growth was fluctuated. Firstly, the microstructural change in the laser welds of Al 6014 alloy is analyzed. High-quality, defect-free welds are successfully produced by ARM laser which can be changed the beam profile freely. An equiaxed structure was formed at the center of the welds, and the equiaxed region compared with fusion zone width was increased as increasing of welding speed. Hot cracking susceptibility was decreased as increasing of equiaxed fraction per unit area. It means that the microstructure formation of the welds affects the hot cracking propagation.

Molten pool size and shape directly influence hot cracking susceptibility. To evaluate the influence of oscillation parameters, laser beam oscillation welding was performed with different beam patterns, widths, and frequencies. The behavior of hot cracking propagation was analyzed by high-speed camera and electron backscatter diffraction. The behavior of crack propagation was observed to be highly correlated with the microstructural evolution of the fusion zone. For an oscillation with an infinite-shaped scanning pattern at 100 Hz and 3.5 m/min welding speed, the bead width, solidification microstructure, and the width of the equiaxed zone at the center of fusion were fluctuating. Furthermore, the equiaxed and columnar regions alternated periodically, which could reduce solidification cracking susceptibility. This originated from the sinuous movement of the laser beam along the longitudinal direction. Consequently, crack propagation was hindered by formation of solidification morphology.

Residual stress at the welds is highly related with the bead appearance. When penetration mode changed from full to partial penetration, length of hot cracking was reduced. To analyze the influence of penetration mode, bead shape factor was analyzed and thermo-mechanical model was developed coupled with the convection heat transfer model. Heat input subjected to the workpiece would affect residual stress behavior during solidification. The strong stress was acted at the bottom place, and it is fairly well agreed with experimental results. From the results, it is confirmed that stress distribution

resulted from variation of penetration mode of the welds affects the hot cracking propagation.

From this study, the effects of thermal cycle and residual stress on hot cracking susceptibility, which has not been clear up to now, is described well. Experimental results and the developed model lead to a clearer understanding about hot cracking propagation during laser welding of aluminum alloy sensitive to hot cracking. These results can be used beneficially to arrange an alternative methodology to avoid hot cracking.

Keywords: Laser welding, Aluminum, 6XXX series Al alloy, Automotive industry, Thin plate, Hot cracking, Hot cracking susceptibility, Temperature gradient (G), Solidification rate (R), Microstructural evolution, Equiaxed grain, Columnar grain, Laser beam profiling, ARM laser, Laser beam oscillation, Oscillation frequency, Oscillation width, Laser beam path, Molten pool behavior, Penetration mode, Full penetration, Partial penetration, Thermo-mechanical modeling, Thermal conduction, Residual stress.

Student number: 2014-31061

Contents

LIST OF TABLES

with lap joint.

Table 4.3 Results of regression analysis between the shape factors and length of crack.

LIST OF FIGURES

between core and ring.

Figure 3.1.3 Images of (a) crack propagation captured by high speed camera during the laser welding, and non-destructive X-ray test specimens of (b) 80 mm/s (c) 100 mm/s and (d) 120 mm/s. The specimen was prepared under a 900 W laser power at the core and 900 W at the ring.

Figure 3.1.4 Crack length measurements with various (a) welding speed and (b) laser power of core. The crack lengths of multi-mode and single-mode laser were illustrated using red line into the graph.

Figure 3.1.5 Macro-section images of laser weldements (a) single-mode (laser power: 900 W, welding speed: 3 m/min); (b) multi-mode (laser power: 1500 W, welding speed: 3 m/min); (c) ARM laser (laser power: 1800W, welding speed: 6 m/min)

Figure 3.1.6 Bead width measurements at the top and bottom surface

according to welding speed and laser power of core. The bead widths of multi-mode and single-mode laser were illustrated using a dash-dot line into the graph.

Figure 3.1.7 Measured molten pool length depending on welding speed using high-speed camera.

Figure 3.1.8 Summary of molten pool behavior with various welding condition. Laser welding was performed under welding speed of 3 m/min and total laser power of 1800 W.

Figure 3.1.9 Microstructure view from the normal direction depending on welding speeds. The laser welding was performed with 900 W of laser power at the core and 900 W of laser power at the ring, while welding speed varied: (a) 80 mm/s; (b) 100 mm/s and (c) 120 mm/s.

Figure 3.1.10 EBSD analysis depending on welding speeds. The dash-dot line refers to the center of the welds and dash line indicated a fusion

line. The specimen was prepared with 900 W of laser power at the core and 900 W of laser power at the ring, while welding speed varied: (a) 80 mm/s; (b) 100 mm/s and (c) 120 mm/s.

Figure 3.1.11 Schematic diagram of the variation of the temperature gradient (G) and solidification rate (R) in chapter 3-1.

Figure 3.2.1 (a) Optical system with a 200-mm focal length (left) and laser power source with a maximum output of 1 kW (right) for oscillating laser beam welding; (b) Schematic image of the self-restraint test specimen to evaluate hot cracking susceptibility.

Figure 3.2.2 Circular and infinite-shaped laser oscillation beam patterns at a welding speed of 3.5 m/min, where w is the oscillation width at 0.8 mm. (a) circular pattern at 100 Hz; (b) circular pattern at 200 Hz; (c) infinite-shaped pattern at 100 Hz; (d) infinite-shaped pattern at 200 Hz.

Figure 3.2.3 Crack length and bead width measurements at the surface according to (a) oscillation width and (b) frequency. Specimen was prepared using a circular scanning pattern under a laser power of 900 W and a welding speed of 3 m/min.

Figure 3.2.4 High-speed camera images of the molten pool during a single oscillation. (a) linear welding with 900 W laser power at 3 m/min welding speed; oscillating laser beam welding with circular pattern and 900 W laser power at 3 m/min welding speed. The oscillation width was fixed at 1.6 mm, while the frequency varied at (b) 100 and (c) 200 Hz.

Figure 3.2.5 EBSD analysis with and without laser beam oscillation. (a) linear welding with 900 W laser power at 3 m/min welding speed; (b) oscillating laser beam welding with circular pattern, 900 W laser power, and oscillation width of 1.6 mm at 200 Hz and 3 m/min welding speed.

Figure 3.2.6 Measured length of the crack from different laser beam scanning patterns and oscillation widths. Specimens were fabricated under 900-W laser power at 200 Hz and 3 m/min welding speed.

Figure 3.2.7 Measured length of the crack for different oscillation widths at varying frequencies. The specimen was prepared with an infinite-shaped pattern and laser power of 900 W at the welding speed of 3.5 m/min.

Figure 3.2.8 Bead appearance view from the normal direction depending on the welding condition (a). Circular scanning pattern with 900 W laser power and 1.6 mm oscillation width at 3 m/min welding speed and 100 Hz oscillation frequency; and (b) infinite-shaped scanning pattern 900 W laser power and 0.4 mm oscillation width at 100 Hz and 3 m/min welding speed.

Figure 3.2.9 High-speed camera images of the molten pool under laser

beam oscillation with an infinite-shaped pattern during a single oscillation. The oscillating laser beam welding was performed with 900 W laser power at 3.5 m/min. The oscillation width was fixed at 0.8 mm, while the frequency varied: (a) 100 and (b) 200 Hz.

Figure 3.2.10 EBSD analysis with varying oscillation frequencies. Welding was performed with infinite-shaped beam pattern under 900 W laser power at 3.5 m/min welding speed. The oscillation width was fixed at 0.8 mm, while the frequency was varied at (a) 0 Hz, (b) 100 Hz, (c) 200 Hz, and (d) 300 Hz.

Figure 3.2.11 Schematic diagram of the molten pool movement, where R represents the local solidification rate, W.D is the welding direction along the x-axis, and Rdt indicates the solid-liquid interface displacement over a time interval.

Figure 3.2.12 FESEM images of the specimens treated with oscillating

laser beams at 100 Hz with the infinite-shaped pattern. (a) Fracture surface 1 mm from the start point; (b) high-magnification image of the yellow box region (i) in Fig. 12(a); and (c) high-magnification image of the yellow box region (ii) in Fig. 12(a).

Figure 4.1 Schematic image of the laser overlapped specimen to evaluate hot cracking susceptibility.

Figure 4.2 (a) Schematic images of active force during the laser welding, and (b) generated crack at the center of a lap fillet joint.

Figure 4.3 Laser oscillation beam patterns circularly at a welding speed of 3 m/min, oscillation width of 0.8 mm and oscillation frequency of (a) 100 Hz; (b) 200 Hz.

Figure 4.4 Bead appearance of the specimen prepared using an oscillation frequency of 200 Hz and oscillation width of (a) 0.2 mm; (b) 0.4 mm; (c) 0.8 mm; and (d) 1.6 mm.

Figure 4.5 (a) Definition of shape factor on section image, and macro-section images (b)-(e) according to the oscillation width. The welding was performed by circular beam pattern under 2300 W laser power, 3 m/min welding speed. The oscillation width was 0.8 mm. (b) 0 Hz; (c) 100 Hz; (d) 200 Hz; (e) 300 Hz.

Figure 4.6 Analysis of bead appearances according to the oscillation width and frequency. (a) bead width at interfacial (a_1); (b) bead width at top surface (a_2); (c) thickness of throat (a_3); (d) bead width at bottom surface (a_4); (e) depth of the welds (a_5); (f): molten area (s_1)

Figure 4.7 Measured crack lengths depending on oscillation width and frequency, which was evaluated by non-destructive X-ray test.

Chapter 1

Introduction

1.1 Growth of the lightweight materials application in automotive industry

In order to respond to the economic and political pressure to reduce fuel consumption and CO_2 emission, the efforts for light weighting in automobile design and constructions have increased significantly. Specific solutions based on the intensive use of aluminum [1-4], magnesium [4], composite [5] as modified or new alloys have been developed in the last decades. Automotive bodies are consists of BIW (Body in White) which is consisted the structure of a vehicle, and hand-on parts such as a door, hood and trunk lid. These parts have a weight of about 30% of the overall weight of a vehicle. Thus, sheet applications for structural parts and BIW construction are gaining interest and efforts have been given by all major producers of semi-finished productions of aluminum alloys to meet the main requirements which are:

- ✓ **Sufficient strength** for structural stability and durability, dent resistance, crash worthiness
- ✓ **Good formability** for stretching, bending and deep drawing operations (including control of anisotropy and spring back)

- ✓ **Joning**, like welding, clinching, glewing, brazing
- ✓ **High corrosion resistance** against filiform, stress induced and contract corrosion
- ✓ **Recyclability** and **low material and fabricating cost**

The principal requirement for many sheet applications is to find the optimum combination of sufficient strength and good formability. For structural parts and for BIW application two main alloy systems used are Al-Mg (5XXX series) and Al-Mg-Si (6XXX) which are well established and typically applied in industry due to their good combination of the required properties. Nowadays, Al-Zn alloy (7XXX series), which was mainly applied to aircraft parts, exhibits a high strength over 500 MPa by the formation of the strengthening precipitates [6] and more recently, research for applying to automobile parts has been progressed [7-9].

1.2 Laser welding: joining techniqure using low heat input by high energy density

The laser was first introduced into the microelectronics industry in the late 1960s for sealing electronic packages and thin-wire connections. At present, laser welding is a proven joining technique in the automotive, metals (parts supply), shipyard, microelectronics, packaging, and aerospace industries [10-12]. In the area of micro-welding, the laser finds many uses in welding of common items such as cigarette lighters, razors, watch springs, motor/transformer lamination, hermetic seals, batteries, and heart pacemakers. [13,14]

A laser has a high-power density heat source. Therefore, 'laser welding' is recognized as an advanced process to join materials with a laser beam of high-power, high-energy density. Consequently, a deep and narrow keyhole is formed during welding compared with arc or plasma welding process. Laser welding can produce a variety of joints of metals and composites even in plastics. It promising joining technology with high quality, high precision, high performance, high speed, good flexibility and low distortion. It can also achieve robotization, reduced manpower, full automation, and systematization in production lines. Applications of laser welding are increasing with the development of novel laser apparatuses and joining processes. Since then

many characteristic lasers such as high-power CO2 lasers, fiber-delivered YAG lasers, and short wavelength Excimer lasers have been utilized in various industries.

1.2.1 Development of laser welding technology

Recently, disk and fiber lasers are expected in terms of high power, high efficiency and high beam quality than that of laser diode pumped YAG laser. Moreover, the disk and fiber lasers are utilized as heat sources for remote welding [15-17]. Remote welding with a robot and scanner is the most promising joining technology of high speed and high production rate. While the scanner optics is being moved in space by the robot which enlarges the scanner's processing space, named as welding-on-the-fly, using synchronization between the motion of the robot axes and the activity of the scanner optics.

In laser welding, a number of defects are frequently observed, such as porosity, surfaces holes or pits, undercuts, humping and solidification cracking. These are deteriorating the quality of the welded parts. Some researchers [18,19] demonstrated that welding defects are related to the keyhole instabilities during the laser welding process. In order to overcome these defects to make high-quality and consistent laser welds, a new welding technique combining two or more laser beam sources, called dual-/multiple-

beam laser welding, has been proposed [20,21] and is under development to become an enabling joining technique for the various materials [22-26].

1.2.2 Comparison between keyhole and conduction laser welding

During the laser welding, there are two main operational regimes can be used: keyhole and conduction laser mode. The main difference between these two modes is the power density. The main characteristics of keyhole laser welding are deep penetration, the small heat affected zone and the high productivity. However, keyhole welding also possesses several problems that may lead to high levels of porosity, instabilities, spatters and other weld defects. Conduction laser welding exhibits several advantages. It allows better control of the heat delivered to the workpiece, and reduced fit-up problems using large beams. However, a penetration depth of conduction mode is shallow, around 2 mm. Advantages and disadvantages of conduction and keyhole laser welding were summarized in Table 1.1.

Table 1.1 Advantages and disadvantages of conduction and keyhole laser welding

Process	Advantage	Disadvantages
Keyhole welding	- Low heat input - Low distortion - Deep penetration - Big aspect ratio - High productivity	- Unstable process - high level of porosity, spatter - Loss of alloying elements - Degradation of mechani-cal properties
Conduction welding	- No vaporization - No porosity, no cracking, no undercut - No spatter - Good gap bridging ability (due to large beam) - Does not require a laser system with a high-quality beam	- Low coupling efficiency - Slow process - High heat input - High distortion

1.3 Thesis motivations: clear understanding about hot crack propagation during laser welding

Aluminum alloy is well known that its lightweight, good formability, and corrosion resistance. Laser welding of aluminum is a challenging due to problems associated with laser welding of aluminum alloy. At first, the high thermal conductivity of aluminum compared to that of carbon steel, which means requiring larger amounts of heat input for welding. Second, low absorptivity causing poor beam energy coupling into the subjected materials. For example, at the temperature below the melting temperature, Nd:YAG laser with a 1,060 nm wavelength has an absorptivity of 0.06. Therefore, the absorptivity normally increases with temperature. In keyhole mode welding, multiple reflections in the keyhole significantly increase energy transfer efficiency. Thus, laser welding has to conduct within the keyhole mode condition. Third, solidification cracking is frequently observed during the laser welding, especially in 2XXX, 6XXX and 7XXX series aluminum alloy. The hot cracking can be easily reduced by adding a filler wire which can e modified the chemical composition of the welds. However, this is not always practical, particularly in laser welding, because additional wire feeding can deteriorate the flexibility of the process.

In order to understand about hot cracking propagation, thermal cycle and

penetration mode were changed and these effects on microstructural and mechanical properties were investigated, too. Because, joint geometries or weld parameter changes that alter the weld bead size and shape are often effective in alleviating cracking.

Thermal cycle during the laser welding high related to welding parameter. Thermal cycle varied molten pool behavior, and it affects the microstructural evolution of the fusion zone. it is very important to understand the microstructural evolution after laser welding because this understanding would enable a prediction of the hot cracking susceptibility. Since the microstructure formation influences hot cracking susceptibility, a good understanding of the relationship between grain structure and hot cracking is necessary. In this study, Laser beam oscillation and multiple beams are suggested as one of the methods to vary thermal cycle, and its effects on hot cracking are explained by analysis of the microstructure of the welds.

In the case of partial penetration mode, it was announced that reduction of length of hot cracking. Therefore, analysis based on changes in the penetration mode and relationship with hot cracking behavior will be discussed. The microstructural evolution of the laser welds and shape factor of the welds which affects hot cracking susceptibility are analyzed, too. These approaches explain well the hot cracking behavior in laser welding under various welding process and joint which has not been clear up to now. In other words, the analyzed results lead to a clear understanding about laser

welding related to hot cracking behavior. Furthermore, this study shows sufficient possibilities, which can predict suppress the hot cracking by selection of welding parameters results in the changing thermal cycle and penetration mode.

1.4 References

[1] Hirsch, J. In Aluminium alloys for automotive application, Materials Science Forum, 1997; Trans Tech Publ: pp 33-50.

[2] Hirsch, J. Aluminium in innovative light-weight car design. Materials Transactions 2011, 52, 818-824.

[3] Hirsch, J. In Automotive trends in aluminium-the european perspective, Materials Forum, 2004; pp 15-23.

[4] Hirsch, J.; Al-Samman, T. Superior light metals by texture engineering: Optimized aluminum and magnesium alloys for automotive applications. Acta Materialia 2013, 61, 818-843.

[5] Stojanović, B.; Ivanović, L. Application of aluminium hybrid composites in automotive industry. Tehnički vjesnik 2015, 22, 247-251.

[6] Dursun, T.; Soutis, C. Recent developments in advanced aircraft aluminium alloys. Materials & Design 2014, 56, 862-871.

[7] Hirsch, J. Recent development in aluminium for automotive applications. Transactions of Nonferrous Metals Society of China 2014, 24, 1995-2002.

[8] Zhou, J.; Wan, X.; Li, Y. Advanced aluminium products and manufacturing technologies applied on vehicles presented at the eurocarbody conference. Materials Today: Proceedings 2015, 2, 5015-5022.

[9] Shin, J.; Kim, T.; Kim, D.; Kim, D.; Kim, K. Castability and mechanical properties of new 7xxx aluminum alloys for automotive chassis/body applications. Journal of Alloys and Compounds 2017, 698, 577-590.

[10] Jasnau, U.; Hoffmann, J.; Seyffarth, P. Nd: YAG–laser–GMA–hybrid welding in shipbuilding and steel construction. In Robotic welding, intelligence and automation, Springer: 2004; pp 14-24.

[11] Chen, H.-C.; Pinkerton, A.J.; Li, L. Fibre laser welding of dissimilar alloys of ti-6al-4v and inconel 718 for aerospace applications. The International Journal of Advanced Manufacturing Technology 2011, 52, 977-987.

[12] Schubert, E.; Klassen, M.; Zerner, I.; Walz, C.; Sepold, G. Light-weight structures produced by laser beam joining for future applications in automobile and aerospace industry. Journal of Materials Processing Technology 2001, 115, 2-8.

[13] Janssen, G. Laser welding in the manufacture of heart pacemakers. Laser Welding, Cutting and Surface Treatment 1984.

[14] Notenboom, G. Laser spot welding in the electronics industry. Laser Welding, Cutting and Surface Treatment 1984.

[15] Sommer, M.; Weberpals, J.-P.; Müller, S.; Berger, P.; Graf, T. Advantages of laser beam oscillation for remote welding of aluminum closely above the deep-penetration welding threshold. Journal of Laser Applications 2017, 29, 012001.

[16] Wang, L.; Gao, M.; Zhang, C.; Zeng, X. Effect of beam oscillating pattern on weld characterization of laser welding of aa6061-t6 aluminum alloy. Materials & Design 2016, 108, 707-717.

[17] Fetzer, F.; Jarwitz, M.; Stritt, P.; Weber, R.; Graf, T. Fine-tuned remote laser welding of aluminum to copper with local beam oscillation. Physics

Procedia 2016, 83, 455-462.

[18] Pastor, M.; Zhao, H.; Martukanitz, R.; DebRoy, T. Porosity, underfill and magnesium lose during continuous wave Nd: YAG laser welding of thin plates of aluminum alloys 5182 and 5754. WELDING JOURNAL-NEW YORK- 1999, 78, 207-s.

[19] Zhou, J.; Tsai, H.-L. Porosity formation and prevention in pulsed laser welding. Journal of Heat Transfer 2007, 129, 1014-1024.

[20] Xie, J. Weld morphology and thermal modeling in dual-beam laser welding. WELDING JOURNAL-NEW YORK- 2002, 81, 283-S.

[21] Xie, J. Dual beam laser welding. Welding journal 2002, 81, 223s-230s.

[22] Chen, W.; Molian, P. Dual-beam laser welding of ultra-thin AA 5052-H19 aluminum. The International Journal of Advanced Manufacturing Technology 2008, 39, 889-897.

[23] Iqbal, S.; Gualini, M.M.; ur Rehman, A. Dual beam method for laser welding of galvanized steel: Experimentation and prospects. Optics & Laser Technology 2010, 42, 93-98.

[24] Pang, S.; Chen, W.; Zhou, J.; Liao, D. Self-consistent modeling of keyhole and weld pool dynamics in tandem dual beam laser welding of aluminum alloy. Journal of Materials Processing Technology 2015, 217, 131-143.

[25] Riahi, M.; Nazari, H. Analysis of transient temperature and residual thermal stresses in friction stir welding of aluminum alloy 6061-T6 via numerical simulation. The International Journal of Advanced Manufacturing Technology 2011, 55, 143-152.

[26] Yan, S.; Hong, Z.; Watanabe, T.; Jingguo, T. CW/PW dual-beam yag laser welding of steel/aluminum alloy sheets. Optics and Lasers in Engineering 2010, 48, 732-736.

Chapter 2

Literature review

Hot cracks are intergranular and interdendritic material imperfections, evolving and growing in a weld pool near zone during execution of a fusion welding process or/and occurs in reheated weld metal during multipass welding. depending on their formation conditions and the locations of their appearance, they can be divided into solidification cracks (SC) in the weld metal and liquation cracks (LC) in the heat affected zone, termed as micro-cracking, miro-fissuring, or HAZ cracking. Classification of hot cracks of these three types was presented in Fig. 1 [1]. Hot cracking resistance was influenced by welding parameters, welding process, alloy composition and restraint conditions of workpieces, respectively, as well as design and metallurgy [2]. These influencing variables are having an interrelation with each other as shown in Fig. 2.

2.1 Literature review: An overview of hot crack formation models

Several hot cracking theories have been advanced. Each of the theories assumes different causes and criteria of hot cracking. Prokhorov [3] postulates the existence of brittle temperature range (BTR), where hot cracking occurs

when a critical strain is reached. Prokhorov's theory determines the hot cracking susceptibility via the relationship between BTR width, ductility, and strain rate $d\varepsilon/dt$.

The rate of feeding (ROF)/ rate of shrinkage mode (ROS), suggested by Feurer [4], is based on the situation of competition between volume shrinkage during solidification and feeding capability of the melt. Thus, Cracking is related to a pressure drop in the interdendritic melt when the melt is incapable of shrinkage feeding

The Rappaz-Drezed-Gremaud (RDG) hot cracking criterion considered that the effect of a local strain perpendicular to the solidification direction caused by external uniaxial stressing [5]. Following Rappaz et al. [5], the RDG model formulated based on a mass balance equation as flow rate vector divergence between the melt inflow and outflow. A relationship is formulated between critical strain rate and melt pressure P, in which solidification crack initiation occurs when P drops below the limit value.

2.2 Literature review: Thermomechanics in weld pool vicinity

A continuative stress-based approach to describe the thermomechanical behavior near the weld pool and the associated hot crack initiation (solidification crack) was presented by Zacharia [6]. The weld pool is

surrounded by a zone of compressive stresses switching over to tensile stresses in a certain property specific distance from the weld pool end, as shown in Fig. 3. The size of the compressive and tensile stress zone can be influenced by a change in welding parameters [6]. Feng et al. mentioned that the welding sequence has a significant influence on the local stress/strain distribution [7,8].

Chihoski [9] states that the welding speed significantly influences the measured strain distribution. He also emphasizes in this paper that a critical tensile stress zone must be existent for hot crack initiation of which the size depends on the welding speed. It was demonstrated that higher welding speeds at simultaneously reduced weld widths and gave increased hot cracking resistance.

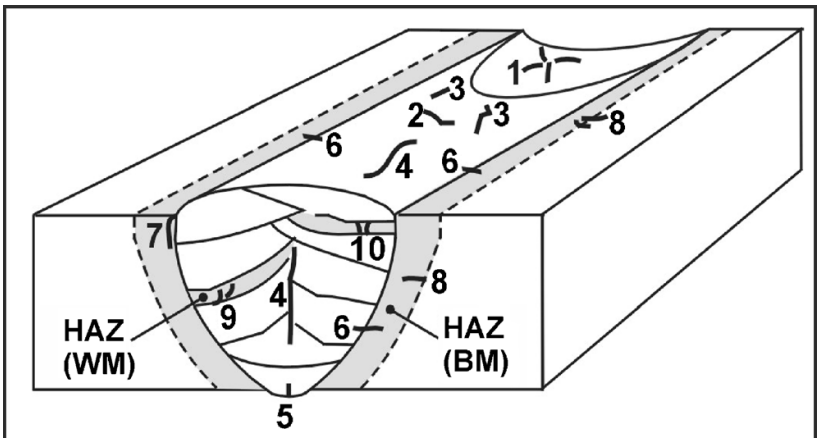

1. Crater crack (SC)	Type 1A	6. Transverse cravk (LC)	Type 1B
2. Transverse crack (SC)	Type 1A	7. Edge crack (LC)	Type 1B
3. Longitudinal Crack (SC)	Type 1A	8. DDC in HAZ	Type 2A
4. Centre crack (SC) in longitudinal section and in transverse section	Type 1A	9. DDC in HAZ (multi-run weld)	Type 2C
5. Root crack (SC)	Type 1A	10. DDC in HAZ (single-run weld)	Type 2B

Fig. 2.1 Designation of hot cracks according to their location in the weld metal (WM) or in the heat-affected zone (HAZ) following [1]

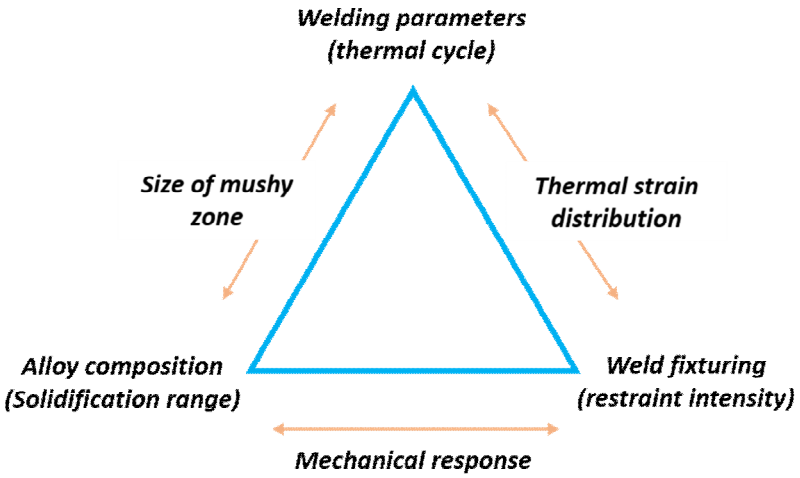

Fig. 2.2 Diagram indicating the complex interaction between process parameters affecting weld solidification cracking [2]

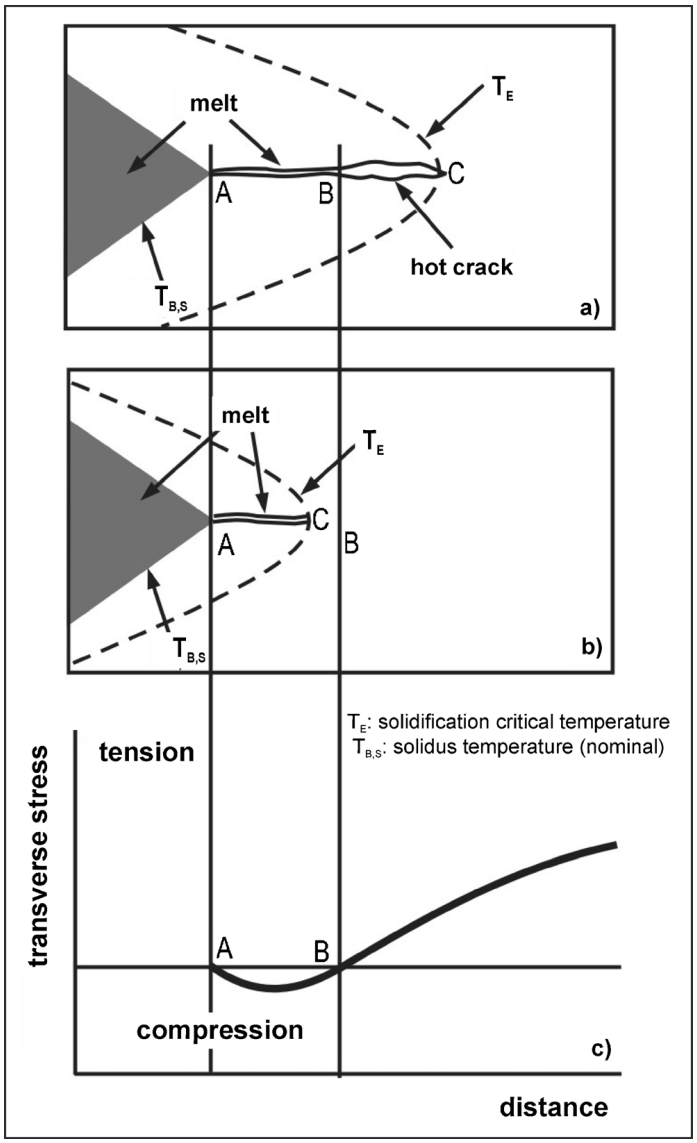

Fig. 2.3 Transverse stress profile depending on a distance from the weld pool end.

2.3 Literature review: An overview of cracking test method with self-restraint

The Houldcroft cracking test [10] called as fishbone-test [11] or keyhole slotted-plate-test, respectively. As shown in Fig. 4, the saw cut depth for the Houldcroft cracking test [10] is gradually increased (decrease in restraint) which entails a continuous change in the local weld pool near strains and strain rates. The restraint force and thermo-mechanical behavior are varied via depending on saw cut depth. In this type of tests, the solidification cracking is usually initiated and propagated along the center of the weld and started from at the narrow edge as shown in Fig. 4.

Self-restraint test is suitable for the investigations of the design-specific hot cracking susceptibility. Shibahara et al. [12] studying the welding direction influence using experimental and numerical investigations. Brooks et al. [13] and Dike et al. [14] discovered strain distribution to be significantly affected by the variable restraint (depending on saw cut depth) during welding with the Houldcroft cracking test. They emphasized that the critical strain is particularly dependent on external loading and specimen shape. Matsuda et al. [15] was performed electron beam welding on aluminum alloy and stainless steels, respectively, and recommended the shape and dimension of the test specimen.

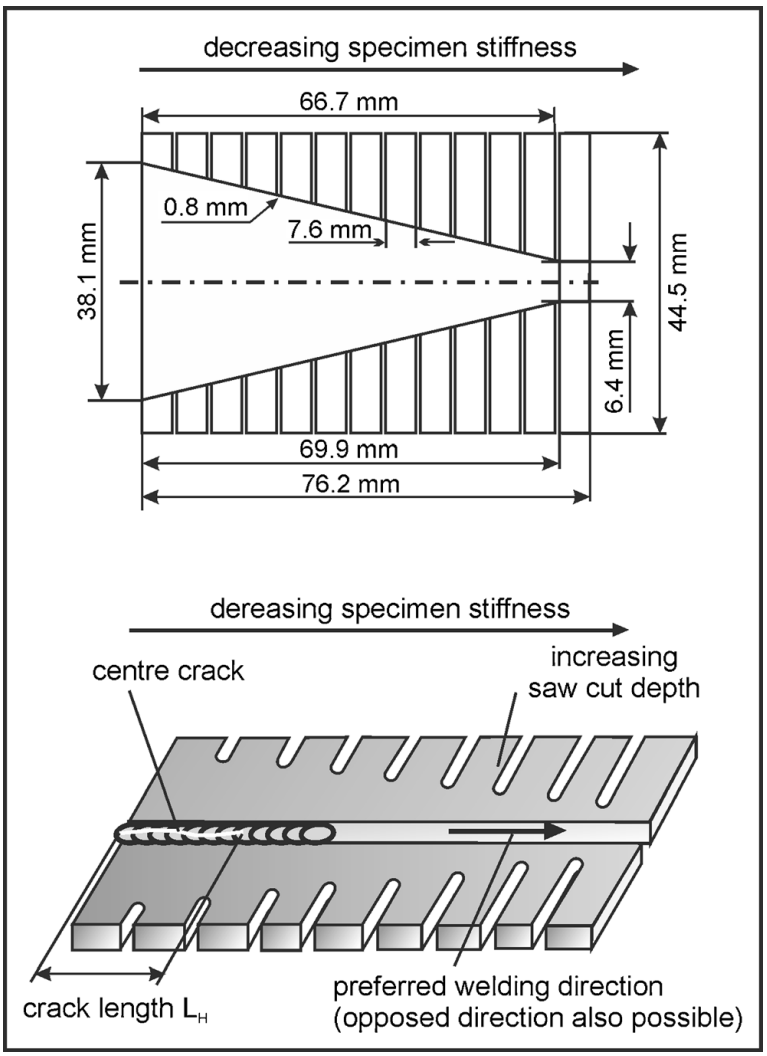

Fig. 4 Schematic diagrams of Houldcroft cracking test specimen [10]

2.4 References

[1] Hemsworth, B.; Boniszewski, T.; Eaton, N. Classification and definition of high-temperature welding cracks in alloys. Metal Construction 1969, 1, 5-16.

[2] Cross, C. On the origin of weld solidification cracking. In Hot cracking phenomena in welds, Springer: 2005; pp 3-18.

[3] PROKHOROV, N. The technological strength of metals while crystallising during welding. Weld. Prod. 1962, 9, 1-8.

[4] Feurer, U. In Influence of alloy composition and solidification conditions on dendrite arm spacing, feeding and hot tearing properties of aluminum alloys, Qual. Control Eng. Alloys Role Met. Sci, Proc. Int. Symp, 1977; pp 131-145.

[5] Rappaz, M.; Drezet, J.-M.; Gremaud, M. A new hot-tearing criterion. Metallurgical and materials transactions A 1999, 30, 449-455.

[6] Zacharia, T. Dynamic stresses in weld metal hot cracking. Welding Journal Including Welding Research Supplement 1994, 73, 164-172.

[7] Feng, Z.; Zacharia, T.; David, S. Thermal stress development in a nickel-based superalloy during weldability test. Welding journal 1997, 76.

[8] Feng, Z.; Zacharia, T.; David, S. In On the thermomechanical conditions for weld metal solidification cracking, 77 th Annual AWS Convention Abstracts, 1996; p 1996.

[9] Chihoski, R.A. The character of stress fields around a weld arc moving on aluminum sheet. Welding Journal 1972, 51, 9.

[10] Houldcroft, P. A simple cracking test for use with argon-arc welding. British Welding Journal 1955, 2, 471-475.

[11] Radhakrishnan, V. Welding technology and design. New Age International: 2005

[12] Shibahara, M.; Serizawa, H.; Murakawa, H. Finite element method for hot cracking using temperature dependent interface element (report ii): Mechanical study of houldcroft test (mechanics, strength & structure design). Transactions of JWRI 2000, 29, 59-64.

[13] Brooks, J.; Dike, J.; Krafcik, J. In On modeling weld solidification cracking, Proceedings of Internal Conference on Modeling and Control of Joining Processes, 1993; pp 174-185.

[14] Dike, J.; Brooks, J.; Krafcik, J. Finite element modeling and verification of thermal-mechanical behavior in the weld pool region; ASM International, Materials Park, OH (United States): 1996.

[15] Matsuda, F.; Nakata, K. A new test specimen for self-restraint solidification crack susceptibility test of electron-beam welding bead: Fan-shaped cracking test Transactions of JWRI 1982, 11, 87-94.

Chapter 3-1

Analysis of hot cracking susceptibility according to thermal cycle induced by laser welding - I (ARM laser)

3.1.1 Introduction:

A new welding technique combining two or more laser beam sources, called dual-/multiple-beam laser welding, has been proposed [1,2] to overcome the formation of defects, such as porosity, undercuts, and solidification. In addition, it can alleviate the fit up the tolerance of workpieces. Presently, the twin-spot laser beam is used when welding galvanized steels, light metals (e.g. aluminum alloys) [3] and when joining steels with non-ferrous metals [4]. Milberg and Trautmann [5,6] and Adam et al. [6] showed that the dual beam laser welding of zinc-coated steels increased the quality of welds.

In dual-beam laser processing, the dual beam can be arranged either side by side or parallel to the welding direction [7,8]. Banas et al. [7] used the bendable mirror to split a laser beam into two beams that were then arranged side by side. They insisted that dual-beam increase the fit up tolerance in

welding tailored blanks. By using dual-beam arranged parallel to the welding direction, it has been reported to provide benefits over conventional single-beam laser welding such as improved weld quality. Xie et al. [2] focused on the dual-beam laser welding processes in terms of cooling rates, and its impact on weld quality was evaluated. Liu et al. [9] performed dual-beam laser welding on AISI 4140 steel. They insisted the beneficial effects resulted in lower cooling rates, reduced hardness, and smaller volume fraction of martensite compared to single-beam laser welds. Kannatey-Asibu [10] developed mathematical models based on the cooling rate in dual-beam laser welding. These theoretical analyses showed the cooling rates at the weld centerline were reduced from 1004 °C/s in the single-beam process to 570 °C/s in the dual-beam process while the laser power and inter-beam spaces were 1.8 kW and 10 mm, respectively.

Laser welded 6XXX series exhibits fine cellular dendrite structure at the center of the fusion zone. Solidification cracking has been observed during the laser of 6XXX series aluminum alloy, which is sensitive to hot cracking. Kang et al. [11] insisted that the behavior of crack propagation correlated with the microstructural evolution of the fusion zone. Ramasamy et al. [12] founded that the weld metal microstructure to be fine cellular dendritic with equiaxed grains increased with increasing travel speed. Venkat et al. [13] performed CO2 laser welding on 5754-O aluminum alloy and insisted that the equiaxed grains observed near the weld centerline at high welding speeds.

Kim et al. [14] performed linear and weaving laser welding on 5XXX series aluminum alloy. They insisted that solidification crack developed along the centreline having equiaxed grains, and calculated temperature gradient and solidification rate to simulate the solidification morphology by finite element method.

Ramasamy et al. [12] mentioned that the cracking was more pronounced at high welding speeds due to the high cooling rates. In addition to the configuration of the joint (lap joint, butt joint, etc.) and the presence of undercuts, humping, cracking, porosity, and other defects also affect the properties of the joints.

In this study, the effect of coaxial shaping dual-beam on hot cracking susceptibility was investigated in high-power laser welding of Al 6XXX series alloy. Moreover, laser welding phenomena depending on welding parameters were examined by observing molten pool behavior. The interaction between welding parameters and formed microstructure into the welds were analyzed, since the microstructure formation influences hot cracking susceptibility.

3.1.2 Experimental procedure for ARM laser welding

A continuou mode Yb:YAG laser was applied to the welding. The laser beam was delivered through an optical fiber with a diameter of 200 μm. The delivered laser beam was irradiated perpendicularly and focused on the surface of the workpiece. During the laser welding, Ar shielding gas was provided through the coaxial nozzle as shown in Fig. 1(a). Laser welding was applied to Al 6014 alloy with a thickness of 1 mm. The specimens were machined as shown in Fig. 1(b) to evaluate the hot cracking susceptibility. The laser welding has begun from the narrow edge and finished the wide edge. The measured chemical compositions and mechanical properties of the applied material are presented in Table 1.

To investigate the influence of the laser beam profile, the laser power at core and ring varied. Figure 2 shows the examples of the laser beam profile. Applied the laser beam consisted of two parts as core and ring. By using the combining module, the beam profile can be varied. The beam at the core and ring had a beam diameter of 52 μm and 230 μm, respectively. Thus, it can switch the beam characteristics similar to the single mode laser, when using the core beam only. If using both of beams at the same time, beam profile shows the characteristics of the multimode laser (Fig. 2). In this study, the power of the core and ring were manipulated in the range of 0 to 1800 W, respectively. The details of the laser welding conditions are summarized in

Table 2.

After welding, a non-destructive X-ray test was conducted to measure the hot cracking length. During welding, the molten pool was observed by a high-speed camera with a diode laser illumination at a rate of 10000 frames per sec. The high-speed camera was tilted by an angle of 45° relative to the specimen. An illumination 808 nm laser of power 100 W and a bandpass filter that transmits radiation in the range 808 nm ± 1.5 nm were used. After the welding, specimens were polished and etched with a NaOH solution to confirm the microstructure, which was observed through an optical microscope.

Table 3.1.1 Chemical compositions measured with ICP analyzer and mechanical properties of applied base material (wt. %)

Chemical compositions (wt. %)								
Si	Fe	Cu	Mn	Mg	Cr	Zn	Ti	Al
0.58	0.21	0.14	0.08	0.64	0.01	0.01	0.03	Bal.

Mechanical properties		
Tensile strength* (MPa)	Yield strength* (MPa)	Elongation at fracture* (%)
234	126	24

*: average of the results of three quasi-static tensile tests.

Table 3.1.2 Laser welding conditions

Laser source	Yb:YAG laser
Laser power (core)	0 ~ 1800 W
Laser power (ring)	0 ~ 1800 W
Welding speed	80 ~ 120 mm/s
Focal position	-1 mm
Shielding gas	N_2, 30 l/min
Beam tilting angle	0°

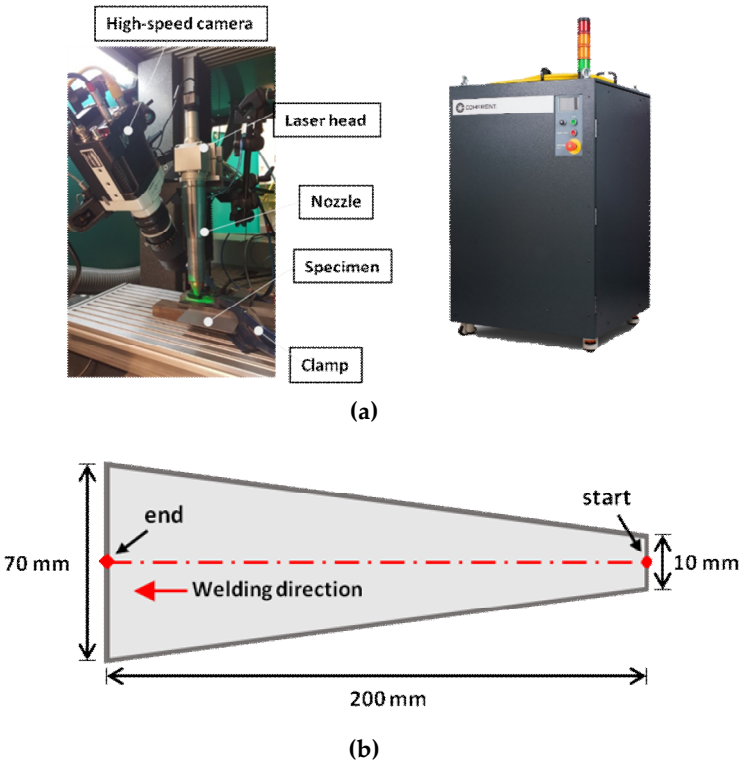

Figure 3.1.1 (a) Experimental setup for laser welding (left) and laser power source with a 2 kW maximum output at the core and 8 kW maximum output at the ring (right); (b) Schematic image of the self-restraint test specimen [15] to evaluate hot cracking susceptibility.

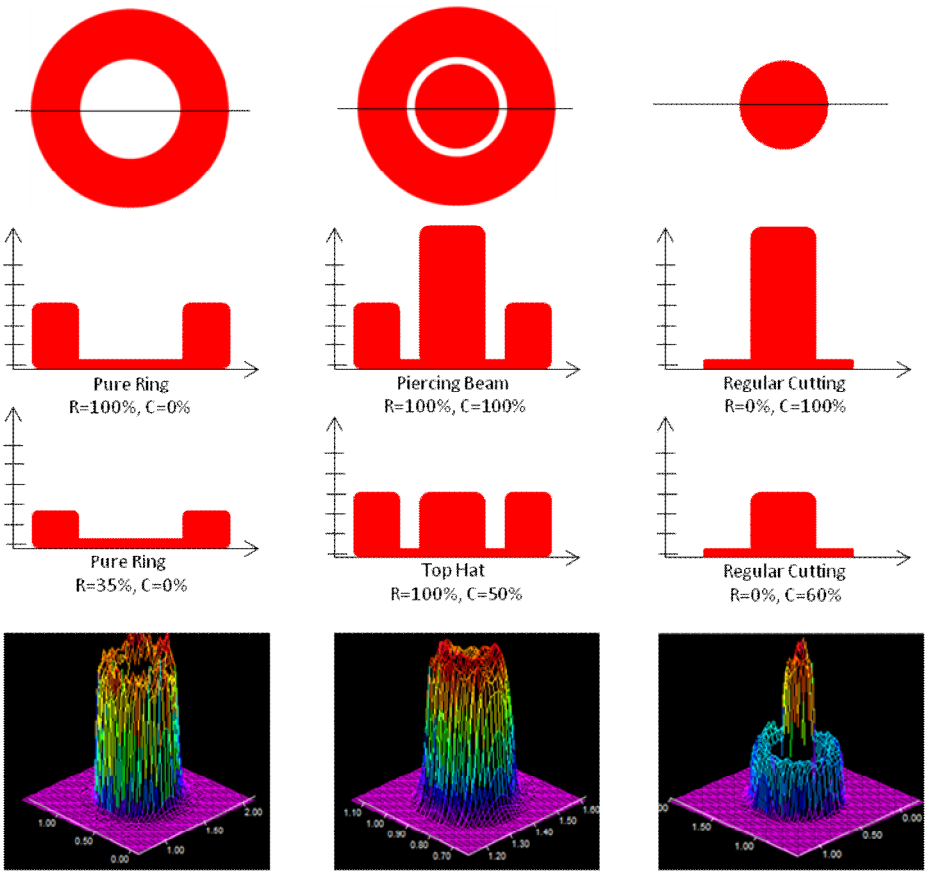

Figure 3.1.2 Beam profiles of ARM laser with various combinations between core and ring.

3.1.3 Effects of beam profiling on laser welding chracteristics

Length of crack was varied according to the welding parameters. The hot cracking was initiated and propagated along the molten pool as shown in Fig. 3(a). As shown in Fig. 3(b), the welding speed affects the crack propagation. Length of cracks was decreased with increasing of welding speed. The crack lengths according to the welding parameters were measured and redrawn in Fig. 3. From the results, it was confirmed that welding speed had a relationship between the lengths of crack (Fig. 3(a)). On the other hand, the correlation between lengths of crack and laser power of core was not obvious (Fig. 3(b)). The crack lengths of lengths of multi-mode and single-mode laser were illustrated using red line into the graph. The measured crack length existed between the crack length of multi-mode and single mode. A configuration of the bead also affect the properties of the joints and hot cracking susceptibility [16]. As shown in Fig. 5, bead appearances were vaired according to the welding parameters. To evaluate the effects of welding parameter on bead appearance, bead width at top (Fig. 6 (a)) and bottom surface (Fig. 6(b)) were measured. Both bead widths affect the welding speed results from reduced the heat input subjected to the specimen. Compared with the multi mode or single mode laser weldments, interval between the width of top and bottom is obvious since the nature of ARM laser beam source. Power

distribution exhibited the shape of bell at the condition of 900 W of laser power at core and 900 W at ring since concentrated enenrgy density at the core compared with the ring part.

The high-speed camera images of molten pool depending on welding parameters can be seen in Fig. 7. Welding speed affects the heat input subjected to the specimen, which changes the molten pool behavior. A longer molten pool was produced at low travel speed condition. Length of the molten pool decreased sharply when high power was applied at the ring part compared with other conditions (Fig. 8).

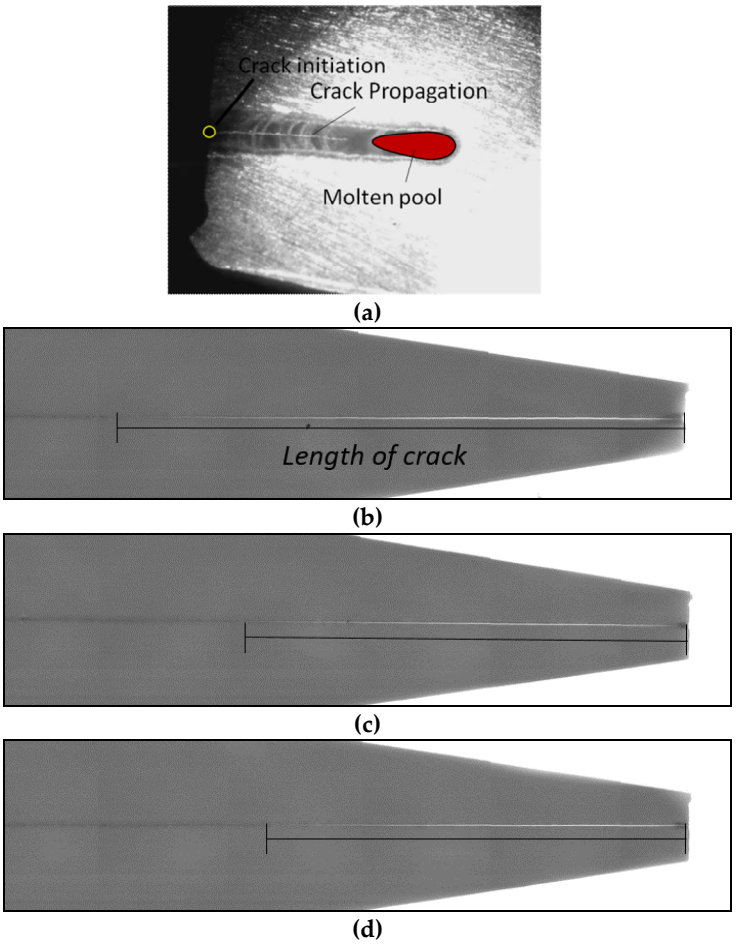

Figure 3.1.3 Images of (a) crack propagation captured by high speed camera during the laser welding, and non-destructive X-ray test specimens of (b) 80 mm/s (c) 100 mm/s and (d) 120 mm/s. The specimen was prepared under a 900 W laser power at the core and 900 W at the ring.

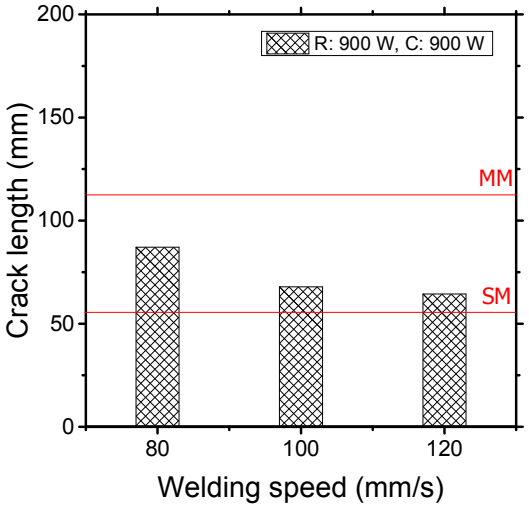

(a)

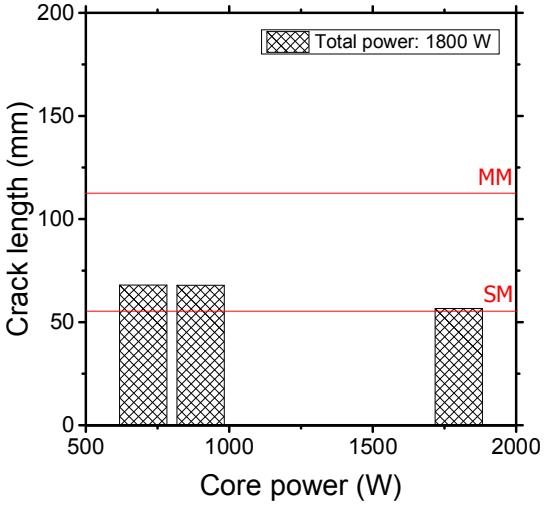

(b)

Figure 3.1.4 Crack length measurements with various (a) welding speed and (b) laser power of core. The crack lengths of multi-mode and single-mode laser were illustrated using red line into the graph.

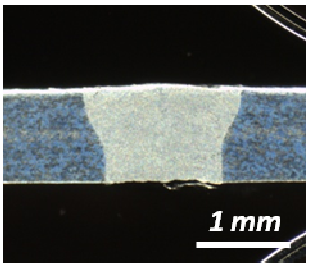

(a)

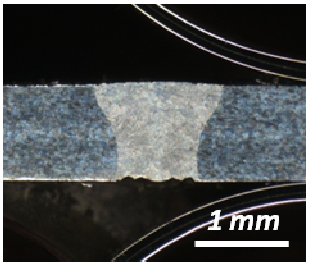

(b)

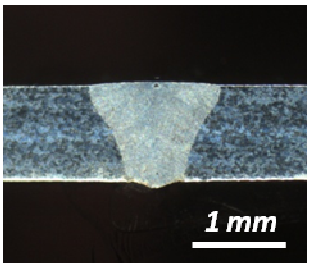

(c)

Figure 3.1.5 Macro-section images of laser weldements (a) single-mode (laser power: 900 W, welding speed: 3 m/min); (b) multi-mode (laser power: 1500 W, welding speed: 3 m/min); (c) ARM laser (laser power: 1800W, welding speed: 6 m/min)

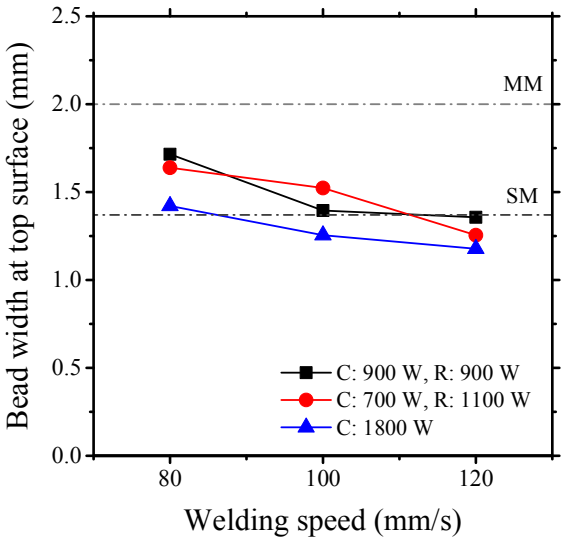
Bead width at top surface (mm)
2.5
2.0
1.5
1.0
0.5
0.0
MM
SM
C: 900 W, R: 900 W
C: 700 W, R: 1100 W
C: 1800 W
80
100
120
Welding speed (mm/s)

(a)

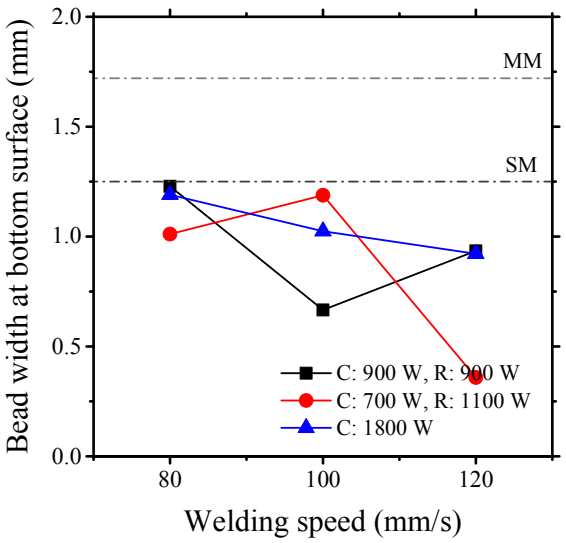
Bead width at bottom surface (mm)
2.0
1.5
1.0
0.5
0.0
MM
SM
C: 900 W, R: 900 W
C: 700 W, R: 1100 W
C: 1800 W
80
100
120
Welding speed (mm/s)

(b)

Figure 3.1.6 Bead width measurements at the top and bottom surface according to welding speed and laser power of core. The bead widths of multi-mode and single-mode laser were illustrated using a dash-dot line into the graph.

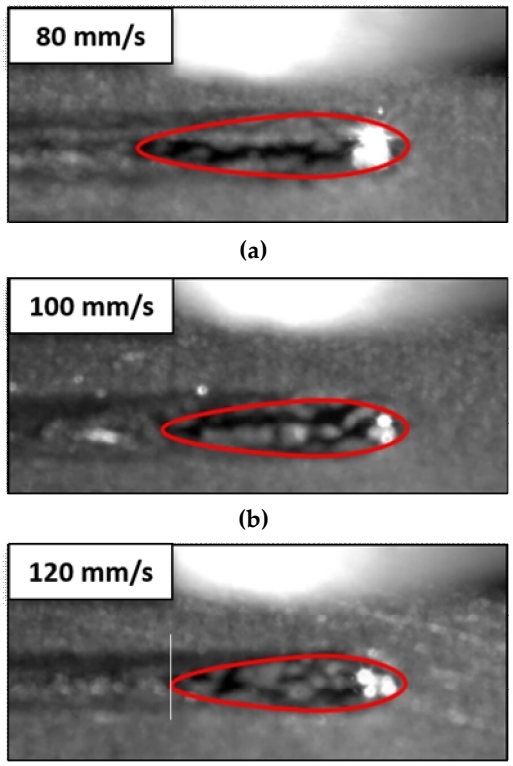

Figure 3.1.7 Measured molten pool length depending on welding speed using high-speed camera.

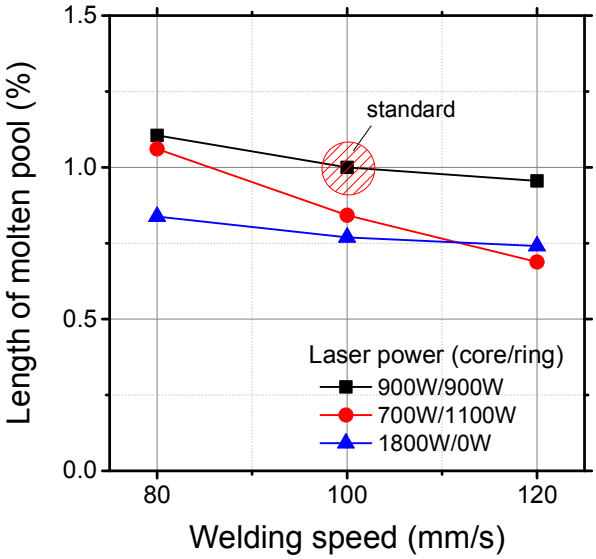

Figure 3.1.8 Summary of molten pool behavior with various welding condition. Laser welding was performed under welding speed of 3 m/min and total laser power of 1800 W.

3.1.4 Effects of beam profiling on microstructural evolution

The crack length decreased with the increasing of welding speed. During the laser welding with self-restrainted specimens, the solidification crack propagated along the centerline. As shown in Fig. 9, symmetrical microstructure formation was confirmed. Wei et al [17] demonstrated that the evolution of microstructure during keyhole mode welding involves several special features such as multiple inflection of weld pool boundary curvatures, strong spatially variable thermal cycle and negligible undercooling by using numerical model. The grain growth direction is determined by the movement of the solid-liquid interface [18-20].

From the normal direction view images, the variation of growth direction did not clear (Fig. 9), but in the EBSD results, the location of the heat source and direction of grain growth can be confirmed (Fig. 10). The equiaxed grain size and region decreased with increasing of welding speed. Dvornak et al. mentioned that fine equiaxed grains are often less susceptible to solidification cracking than coarse columnar grains [21,22]. In the specimen with low welding speed, coarsen equiaxed grain was formed at the center of the welds (Fig. 10 (a)), and small equiaxed grain was observed where in weldments with relatively fast welding speed (Fig. 10(c)). At higher welding speed condition,

solidification rate is faster compared with lower welding speed condition. As shown in Fig. 11, fast solidification rate enhanced the formation of equiaxed structure, but the columnar structure consisted the welds at high welding speed. This means that temperature gradient affects the microstructural evolution. The temperature gradient is defined as the temperature variation per unit length. However, temperature variation between solidus and liquidus temperature cannot be varied, but the distance was affected by welding parameters. Thus, if the local temperature gradient was enough high due to short cooling duration, then a columnar microstructure can be generated.

Fine equiaxed grains can deform to accommodate contraction strains more easily, than columnar grains. However, the crack propagation hindered by grain growth due to it is perpendicularly to the cracking propagation direction. The hot cracking propagated along the center of welds. Thus, the constituent phase and size of the structure at centerline should be considered to suppress the crack because it can determine the crack propagation path.

Applied heat input affects the molten pool dynamic and solidification behavior. At upper part irradiated with heat source was solidified lastly, since the molten pool was elongated resulted from welding speed. Applied beam profile as heat source also influenced aspect ratio (width over length) of molten pool depending on welding parameters. Without the presence of stress acting on adjacent grains during solidification, no cracking can occur. Bead shape also affects hot cracking propagation, which can be varied the direction

of force generated during the solidification. In this experiment, the crack propagated along the equiaxed region, and the longest crack length was measured under coarsen equiaxed condition with I-butt shape bead. It was confirmed that the correlation of constituent structure on the cracking propagation path and hot cracking.

(a)

(b)

(c)

Figure 3.1.9 Microstructure view from the normal direction depending on welding speeds. The laser welding was performed with 900 W of laser power at the core and 900 W of laser power at the ring, while welding speed varied: (a) 80 mm/s; (b) 100 mm/s and (c) 120 mm/s.

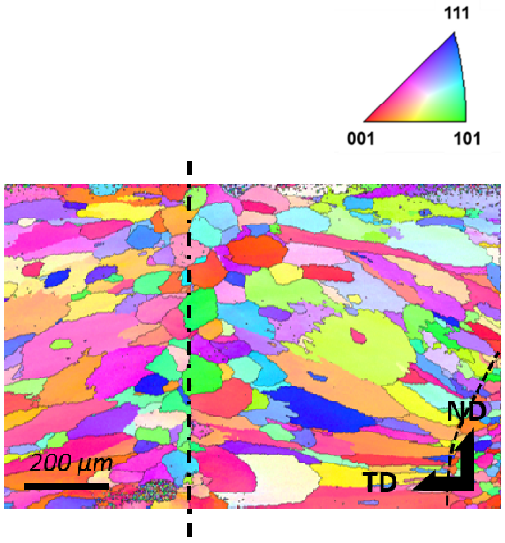

(a)

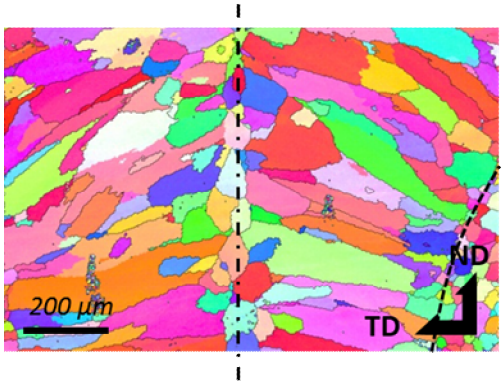

(b)

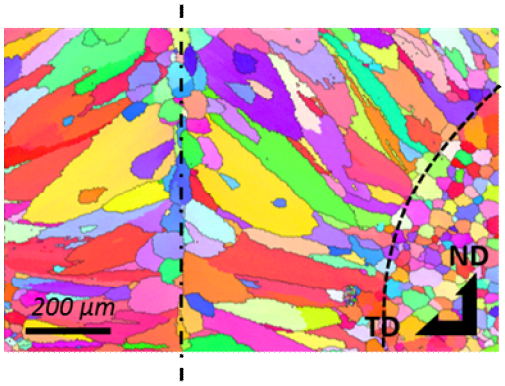

(c)

Figure 3.1.10 EBSD analysis depending on welding speeds. The dash-dot line refers to the center of the welds and dash line indicated a fusion line. The specimen was prepared with 900 W of laser power at the core and 900 W of laser power at the ring, while welding speed varied: (a) 80 mm/s; (b) 100 mm/s and (c) 120 mm/s.

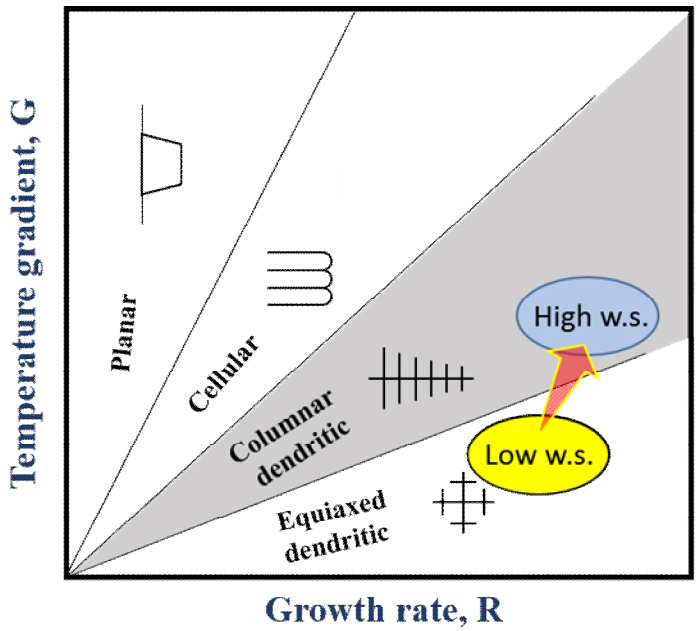

Figure 3.1.11 Schematic diagram of the variation of the temperature gradient (G) and solidification rate (R) in chapter 3-1.

3.1.5 Conlusions

In this study, a self-restraint test was conducted by applying an ARM laser capable of varying beam profile to aluminum 6014 alloy, which is applied in the automotive industry, and evaluated hot cracking susceptibility. The small beam located at the core of ARM laser was beneficial to create the keyhole, and ring beam located at the outside of core beam contributed to changing the bead shape to bell shape instead of common I-butt shape.

Laser welded 6XXX series exhibits fine equiaxed structure at the center of the fusion zone. Solidification cracking has been observed at the center of the welds during the laser of 6XXX series aluminum alloy, which is sensitive to hot cracking. Length of cracking was varied with the welding parameters. Measure crack length was similar to that of a single mode laser, but the width of a bead at the top was wider than single mode. This means that the heat input applied to the ring module can release the fitup tolerance.

Where the longest crack occurs conditions, the equiaxed structure at the center of the welds was coarse and the exhibited and I-butt shape. Grain coarsening can promote the propagation of cracks because it caused a simplification of the crack propagation path. The shape of welds correlated with the behavior of the molten pool. At high welding speeds, the shape of beads was bell type similar with the shape of the heat source of ARM laser. Depending on the bead shape and constituting phase into the welds, the

direction of the shrinkage force during the cooling process can be varied, and these factors can also affect the cracking behavior. Consequently, crack propagation was hindered by this solidification morphology constituting the fusion zone.

3.1.6 References

[1] Xie, J. Weld morphology and thermal modeling in dual-beam laser welding. WELDING JOURNAL-NEW YORK- 2002, 81, 283-S.

[2] Xie, J. Dual beam laser welding. Welding journal 2002, 81, 223S-230S.

[3] Pang, S.; Chen, W.; Zhou, J.; Liao, D. Self-consistent modeling of keyhole and weld pool dynamics in tandem dual beam laser welding of aluminum alloy. Journal of Materials Processing Technology 2015, 217, 131-143.

[4] Yan, S.; Hong, Z.; Watanabe, T.; Jingguo, T. CW/PW dual-beam yag laser welding of steel/aluminum alloy sheets. Optics and Lasers in Engineering 2010, 48, 732-736.

[5] Milberg, J.; Trautmann, A. Defect-free joining of zinc-coated steels by bifocal hybrid laser welding. Production Engineering 2009, 3, 9-15.

[6] Grajcar, A.; Morawiec, M.; Różański, M.; Stano, S. Twin-spot laser welding of advanced high-strength multiphase microstructure steel. Optics & Laser Technology 2017, 92, 52-61.

[7] Banas, C.M.; Doyle, B.M. Twin spot laser welding. Google Patents: 1987.

[8] ARATA, Y.; NABEGATA, E. Tandem electron beam welding (report-i). Transactions of JWRI 1978, 7, 101-109.

[9] Liu, Y.-N.; Kannatey-Asibu, E. Laser beam welding with simultaneous

gaussian laser preheating. Journal of heat transfer 1993, 115, 34-41.

[10] Kannatey-Asibu, E. Thermal aspects of the split-beam laser welding concept. Journal of engineering materials and technology 1991, 113, 215-221.

[11] Kang, M.; Han, H.; Kim, C. Microstructure and solidification crack susceptibility of al 6014 molten alloy subjected to a spatially oscillated laser beam. Materials 2018, 11, 648.

[12] Ramasamy, S. Co2 and nd: Yag laser beam welding of 6111-T4 and 5754-o aluminum alloys for automotive applications. The Ohio State University, 1997.

[13] Venkat, S.; Albright, C.; Ramasamy, S.; Hurley, J. CO_2 laser beam welding of aluminum 5754-O and 6111-T4 alloys. 1997.

[14] Kim, C.; Kang, M.; Kang, N. Solidification crack and morphology for laser weave welding of al 5J32 alloy. Science and Technology of Welding and Joining 2013, 18, 57-61.

[15] Matsuda, F.; Nakata, K. A new test specimen for self-restraint solidification crack susceptibility test of electron-beam welding bead: Fan-shaped cracking test Transactions of JWRI 1982, 11, 87-94.

[16] Dan, W.; Shuntaro, S.; Kota, K.; Kenji, S.; Motomichi, Y. Investigation of evaluation method for hot cracking susceptibility of 310S stainless steel during laser welding using trans-varestraint test. Quarterly Journal of the Japan Welding Society 2015, 33, 39s-43s.

[17] Wei, H.; Elmer, J.; DebRoy, T. Crystal growth during keyhole mode laser welding. Acta Materialia 2017, 133, 10-20.

[18] David, S.; Vitek, J. Correlation between solidification parameters and weld microstructures. International Materials Reviews 1989, 34, 213-245.

[19] Kou, S. Welding metallurgy. Second ed.; John Wiley & Sons: New York, USA, 2002.

[20] Wei, H.; Elmer, J.; DebRoy, T. Three-dimensional modeling of grain structure evolution during welding of an aluminum alloy. Acta Materialia 2017, 126, 413-425.

[21] Dvornak, M.; Frost, R.; Olson, D. Influence of solidification kinetics on aluminum weld grain refinement. Welding Journal 1991, 70, 271s-276s.

[22] NAKATA, K.; MATSUDA, F. Evaluations of ductility characteristics and cracking susceptibility of Al alloys during welding (materials, metallurgy & weldability). Transactions of JWRI 1995, 24, 83-94.

Chapter 3-2

Analysis of hot cracking susceptibility according to thermal cycle induced by laser welding - II (laser beam oscillation)

This journal paper was published in the Materials, titled “Microstructure and solidification crack susceptibility of Al 6014 molten alloy subjected to a spatially oscillated laser beam”. The research for the paper was performed with Dr. Cheolhee Kim, Professor Heung Nam Han.

In terms of the co-author involvement, Dr. Cheolhee Kim and Professor Heung Nam Han assisted with defining the scope of the hot cracking. The experimental work, including the high-speed video observation of the molten pool, were performed by the Sanghoon Kang and author of this thesis. The author carried out most of analyses and discussion. Relating the cracking to the behavior of molten pool was the idea of the Dr. Cheolhee Kim.

Microstructure and solidification crack susceptibility of Al 6014 molten alloy subjected to a spatially oscillated laser beam

Minjung Kang[1,2], Heung Nam Han[2] and Cheolhee Kim[1,*]

[1] Welding and Joining Research Group, Korea Institute of Industrial Technology, 7-47, Songdodong, Yeonsugu, Incheon 21999, South Korea
[2] Department of Materials Science and Engineering and RIAM, Seoul National University, Seoul 08826, Korea
[*] Corresponding: chkim@kitech.re.kr; Tel: +82-32-850-0222; Fax: +82-32-850-0210

Abstract: Oscillating laser beam welding for Al 6014 alloy was performed using a single mode fiber laser and two-axis scanner system. Its effect on the microstructural evolution of the fusion zone was investigated. To evaluate the influence of oscillation parameters, self-restraint test specimens were fabricated with different beam patterns, widths, and frequencies. The behavior of hot cracking propagation was analyzed by high-speed camera and electron backscatter diffraction. The behavior of crack propagation was observed to be highly correlated with the microstructural evolution of the fusion zone. For most oscillation conditions, the microstructure resembled that of linear welds. A columnar structure was formed near the fusion line and an equiaxed structure was generated at its center. The wide equiaxed zone of oscillation welding increased solidification crack susceptibility. For an oscillation with an infinite-shaped scanning pattern at 100 Hz and 3.5 m/min

welding speed, the bead width, solidification microstructure, and the width of the equiaxed zone at the center of fusion were fluctuating. Furthermore, the equiaxed and columnar regions alternated periodically, which could reduce solidification cracking susceptibility.

Keywords: Laser welding; single mode laser; beam oscillation; Al alloy; solidification cracking susceptibility; microstructure; solidification morphology

3.2.1 Introduction

Solidification cracking is a well-known defect frequently observed in aluminum welds. The low ductility of a semi-solid in the mushy zone and the high solidification shrinkage of aluminum alloys both increase hot cracking susceptibility [1, 2]. Solidification cracking is initiated by complex interactions between metallurgical and mechanical factors [3]. During laser welding, this can be diminished by improving chemical composition, refining solidification structure, optimizing laser pulsing parameters, and/or reducing thermal strains [4]. The chemical composition of welds can be easily improved by adding a filler wire, a method utilized in arc welding processes to reduce solidification cracking. However, this is not always practical, particularly in laser welding, because additional wire feeding can deteriorate the flexibility of the process.

Solidification cracking has been evaluated for various fusion welding

processes such as arc welding [5-7], electron beam welding [8], and laser beam welding [9-12]. Laser welding using a high-density laser beam can reduce heat input to a workpiece and minimize thermal distortion. Recently, a high-speed laser beam oscillation technique using galvanometric scanners was developed, allowing the use of wide weld beads and controlling the thermal history of welds. Process flexibility is also guaranteed by a high moving speed with a small heat input. Its application to industrial materials such as steel [13, 14], aluminum [15-18], and copper [19] has been attempted. The use of dynamic oscillation techniques leads to the stabilization of the welding process in terms of welding depth and molten pool behavior [15]. Laser beam oscillation regulates the shape of heat flow, temperature gradient, and solidification rate [20]. Wang et al. controlled the fraction of equiaxed microstructure in the fusion zone by applying laser beam oscillation [21]. A single mode laser with high brilliance is gradually being applied in welding. The high energy density of a single mode laser beam enhances the laser scan speed and oscillation frequency, which could have unique applications [22, 23]. Previous studies have demonstrated how laser beam oscillation affected weld morphology. However, the influence of high speed beam oscillation on hot cracking susceptibility is still insufficiently discussed.

Kou and Le [24] suggested that modifying the microstructure by welding arc oscillation hindered solidification cracking. The direction of columnar dendritic grains changed periodically with the heat source oscillation, which

made crack propagation difficult. Gollnow et al. [25] reported that the angle between the fusion line and the predominant main axis grains is correlated to the probability of occurrence of hot cracking. Shinozaki et al. [26] suggested that a coarse equiaxed grain structure resulted in high solidification cracking susceptibility, which was also confirmed by Tang and Vollertsen [27]. They added the AlTi5B1 alloy in the weld metal to refine its grains and observed that an optimum grain size minimized cracking susceptibility. Witzendorf et al. [28, 29] evaluated the effects of relevant solidification parameters like temperature gradient and local grain growth rate during pulse laser welding. They insisted that the interface velocity (solidification rate) significantly influences hot cracking susceptibility since the temperature gradient at the final stage of solidification was hardly affected by other process parameters. Using a multimode laser with a beam diameter of 0.6 mm, Choi et al. [30] applied a low-frequency laser oscillation on the 6K21 Al alloy to improve its joint strength. The solidification crack was minimized at an oscillation frequency of 5 Hz. However, the molten pool overlapped at 20 Hz, and the joining strength degraded. Consequently, Kim et al. [31] developed a numerical analysis model to predict the morphology in low-frequency laser oscillation welding.

Since the microstructure formation influences hot cracking susceptibility, a good understanding of the relationship between grain structure and hot cracking is necessary. In this study, laser beam oscillation for the welding of

Al 6014 alloy was performed with a single mode laser and a beam scanning system. Its effect on the microstructural evolution of the fusion zone and hot cracking susceptibility were investigated.

3.2.2 Experimental procedure for laser bema oscillation

For the welding process, a single mode Yb:YAG laser, YLR-1000-SM-WC (IPG Photonics, Oxford, MA, USA), was used. The laser beam was delivered through an optical fiber with a diameter of 13 μm. The path was implemented by a single-axis translation system and two-axis beam scanner, D50 (IPG Photonics, Oxford, MA, USA), with a focal length of 250 mm (Fig. 1(a)). The laser beam was perpendicularly irradiated to the specimen and was focused on the upper surface of the workpiece with a beam diameter of 41 μm. A shielding gas was not present during welding. To evaluate the hot cracking susceptibility under different welding conditions, a self-restraint test specimen was fabricated (Fig. 1(b)) [8]. Laser welding initiated at the narrow edge and ended at the wide one. The dimensions of the specimen are shown in Fig. 1(b). The base material was a 1 mm-thick Al 6014-T4 alloy. The chemical composition of the base material is shown in Table 1.

The beam scanner, equipped with two galvanometers to rotate the mirrors, can generate various oscillation patterns. In this study, circular and infinite-shaped patterns were adopted instead of general linear motion. To investigate the influence of laser beam oscillation, the oscillation width and frequency were varied. Figure 2 shows the laser beam path for the circular and infinite-shaped beam patterns at different frequencies. The single-axis

translation system linearly moves the scanner along the x-axis, with a fixed travel speed (welding speed). The laser beam path is determined by considering the position of the scanner and the two-dimensional beam motion (circle or infinite-shaped) of the scanner. The details of the laser welding conditions are presented in Table 2. After welding, a non-destructive X-ray test was conducted to measure the hot cracking length using XSCAN-H160 (XAVIS, Seongnam, Gyeonggi, Korea). During welding, the molten pool surface was observed by a high-speed camera UX50 (Photron, San Diego, CA, USA) with a diode laser illumination LIMO120-F400 (Limo, Bookenburgweg, Dortmund, Germany) at a rate of 2000 frames/sec. The high-speed camera was tilted by an angle of 80° relative to the specimen. An illumination 808 nm laser of power 100 W and a bandpass filter that transmits radiation in the range 808 nm ± 1.5 nm were used.

After welding, horizontally sectioned specimens were prepared for microstructure observation. These were polished and etched with a solution of 1 ml HF, 1.5 ml HCl, 2.5 ml HNO3, and 95 ml H2O. The microstructure of the welds was observed through field-emission scanning electron microscopy (FESEM), using a Quanta 200 F (FEI company, Hillsboro, OR, USA), with electron backscatter diffraction (EBSD), using a Digiview4 (EDAX, Mahwah, NJ, USA). The EBSD specimens were mechanically polished, and then electro-polished at room temperature in a solution of 10% perchloric acid and

ethanol at an operating voltage of 22 V. The critical misorientation angle was set at 15° for grain identification. The data were interpreted using an orientation imaging microscopy analysis software.

Table 3.2.1 Chemical compositions measured with ICP analyzer and mechanical properties of applied base material (wt. %)

Chemical compositions (wt. %)								
Si	Fe	Cu	Mn	Mg	Cr	Zn	Ti	Al
0.58	0.21	0.14	0.08	0.64	0.01	0.01	0.03	Bal.

Mechanical properties		
Tensile strength* (MPa)	Yield strength* (MPa)	Elongation at fracture* (%)
234	126	24

*: average of the results of three quasi-static tensile tests.

Table 3.2.2 Laser welding conditions

Laser power	900 W
Welding speed	3 m/min ~ 3.5 m/min
Oscillation width	0 ~ 1.6 mm
Oscillation frequency	0 ~ 300 Hz
Beam pattern	Linear, Circle, Infinite-shaped
Shielding gas	Non-shielding
Focal position	0 mm
Beam tilting angle	0°

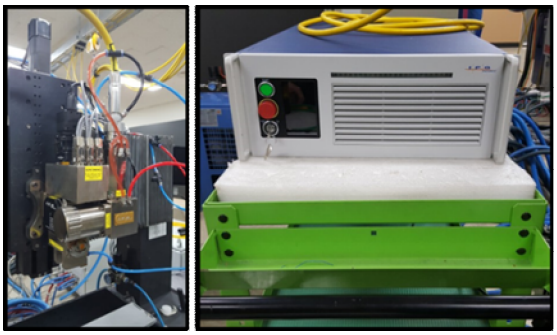

(a)

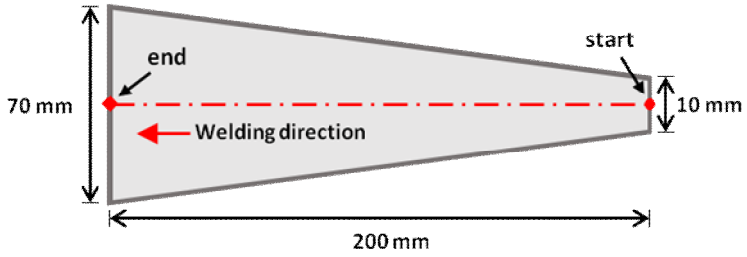

(b)

Figure 3.2.1 (a) Optical system with a 200-mm focal length (left) and laser power source with a maximum output of 1 kW (right) for oscillating laser beam welding; (b) Schematic image of the self-restraint test specimen [8] to evaluate hot cracking susceptibility.

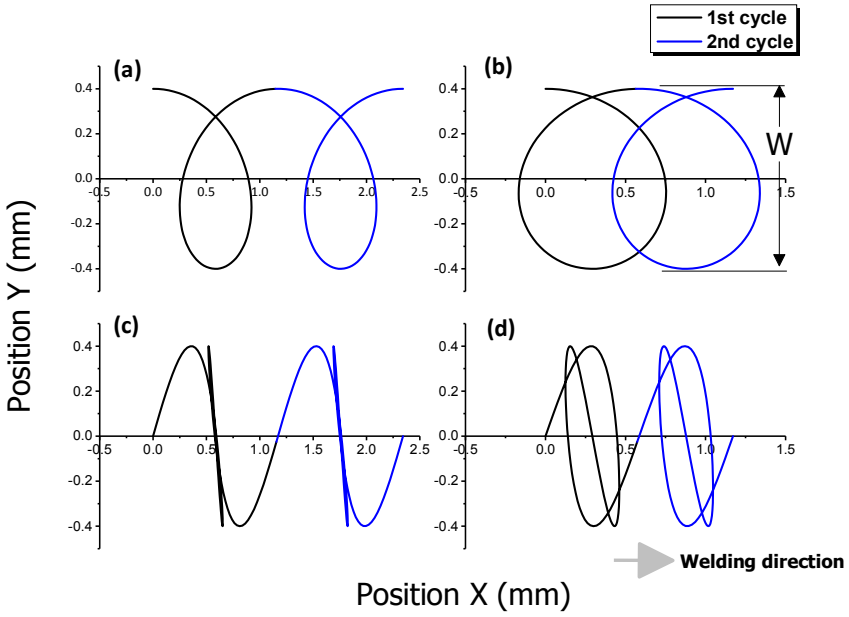

Figure 3.2.2 Circular and infinite-shaped laser oscillation beam patterns at a welding speed of 3.5 m/min, where w is the oscillation width at 0.8 mm. (a) circular pattern at 100 Hz; (b) circular pattern at 200 Hz; (c) infinite-shaped pattern at 100 Hz; (d) infinite-shaped pattern at 200 Hz.

3.2.3 Effects of circular beam pattern on hot crack susceptibility

Oscillation width and frequency affected the hot cracking behavior. After welding with a circular beam pattern, longer cracks were observed at higher oscillation widths (Fig. 3(a)). The width of the molten pool increased with the oscillation width. However, upon increasing the oscillation frequency, the hot cracking behavior varied. With an oscillation width of 1.6 mm, the longest crack was obtained at 100 Hz. Beyond this frequency, the length of the crack decreased correspondingly (Fig. 3(b)). This confirmed the correlation of crack length with the bead width.

Molten pool size and shape directly influence hot cracking susceptibility [32]. The high-speed images of the molten pool for the circular beam scanning pattern can be seen in Fig. 4. Both oscillation width and frequency affect the heat input to the specimen, which changes the molten pool behavior. The location of the keyhole and its moving direction are indicated by the red dot and arrow, respectively. Compared to linear welding (Fig. 4(a)), a wider molten pool was produced by the oscillating laser beams (Figs. 4(b) & 4(c)). A small keyhole generated by a single mode laser beam rapidly spins within the molten pool. However, the shape of the molten pool remained almost uniformly independent of the keyhole position. At the solidification boundary on the surface, the grain growth rates (R) and welding speed were equal at

various oscillation frequencies, but the temperature gradient (G) was slightly different. Accordingly, the microstructural evolution within the welds due to the circularly oscillated beam was similar to that within the linear weld (Fig. 5(a)). The columnar structure formed near the fusion line, while the equiaxed structure was generated at the center of the fusion zone. Furthermore, the resulting equiaxed zone was wider (Fig. 5(b)) than that in the linear weld, because the temperature gradient is less in the circular patterns, which promotes the formation and growth of equiaxed structures [33]. The wide equiaxed zone along the centerline promoted the propagation of solidification cracks during welding [31]. Hence, the length of the crack increases with the oscillation width, as shown in Fig. 3(a). At high oscillation frequencies, the molten pool contracted (Fig. 3(b)), which resulted in the reduction of solidification cracks.

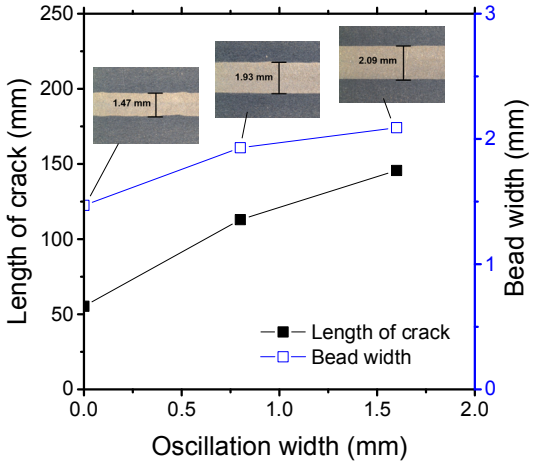

(a)

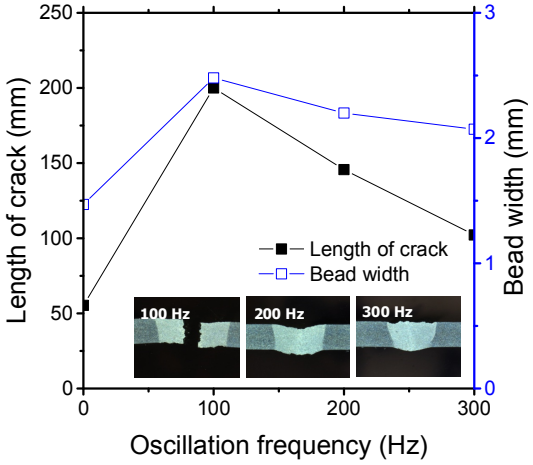

(b)

Figure 3.2.3 Crack length and bead width measurements at the surface according to (a) oscillation width and (b) frequency. Specimen was prepared using a circular scanning pattern under a laser power of 900 W and a welding speed of 3 m/min.

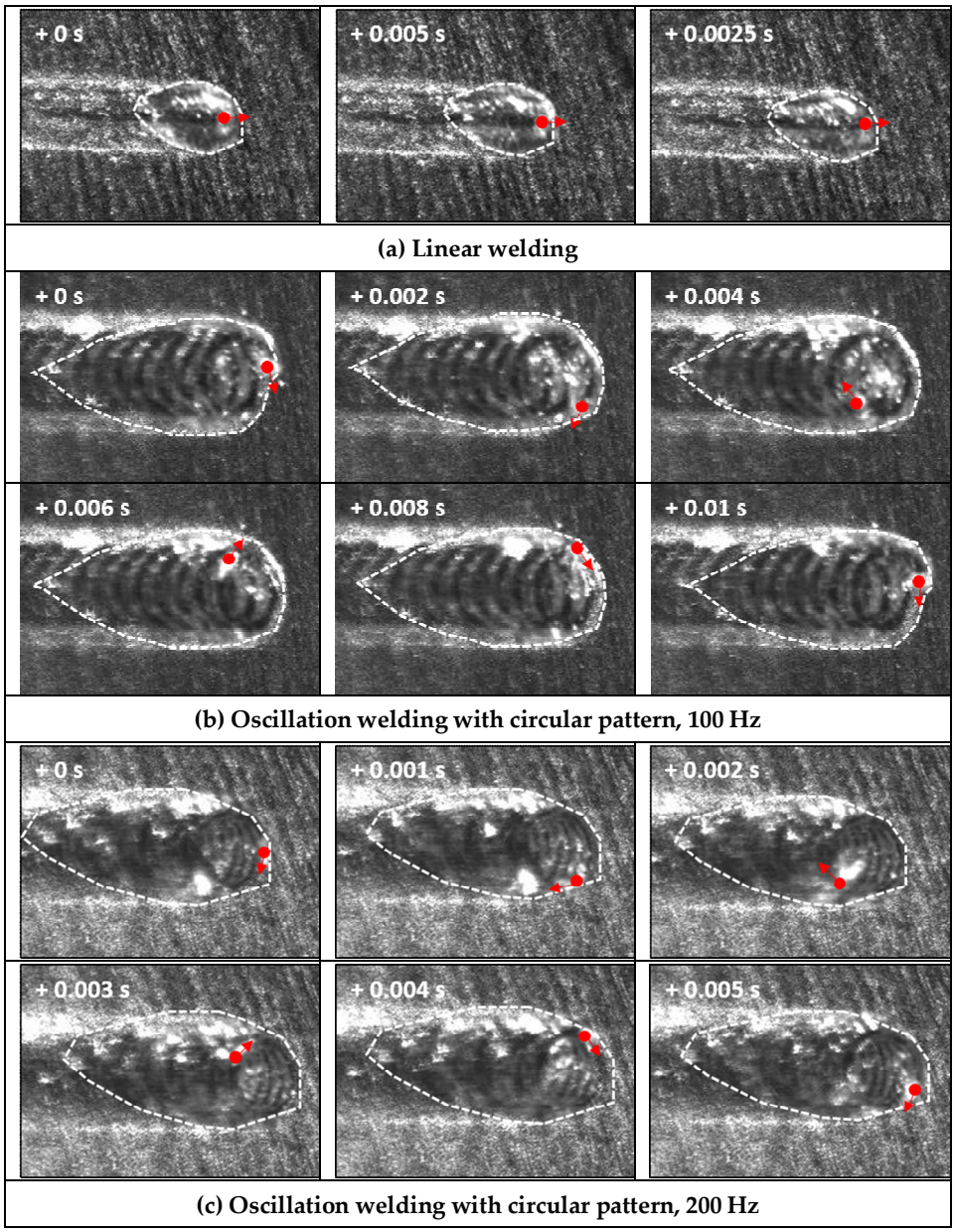

Figure 3.2.4 High-speed camera images of the molten pool during a single oscillation. (a) linear welding with 900 W laser power at 3 m/min welding

speed; oscillating laser beam welding with circular pattern and 900 W laser power at 3 m/min welding speed. The oscillation width was fixed at 1.6 mm, while the frequency varied at (b) 100 and (c) 200 Hz.

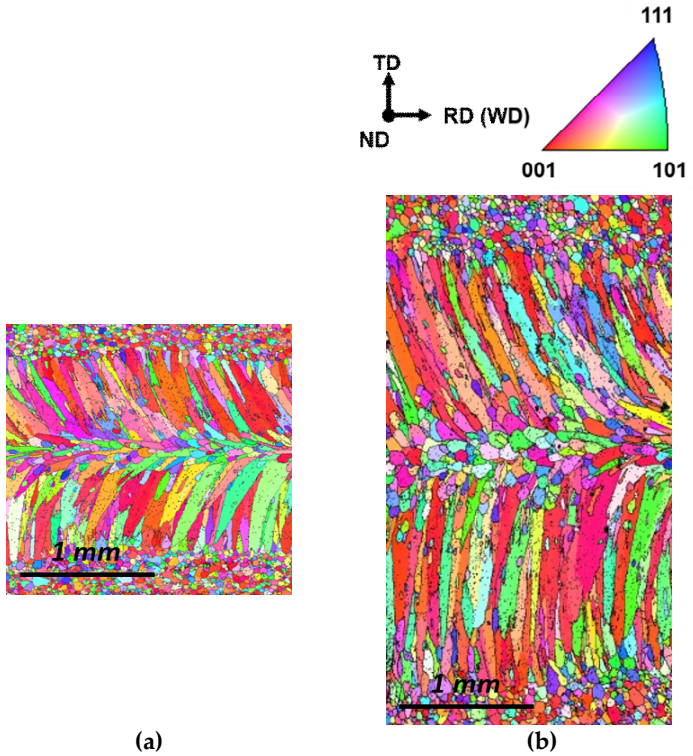

Figure 3.2.5 EBSD analysis with and without laser beam oscillation. (a) linear welding with 900 W laser power at 3 m/min welding speed; (b) oscillating laser beam welding with circular pattern, 900 W laser power, and oscillation width of 1.6 mm at 200 Hz and 3 m/min welding speed.

3.2.4 Effects of infinite beam pattern on hot crack susceptibility

The cracking behavior for the infinite-shaped beam oscillation was similar to that for the circular beam oscillation. The crack length increased with the oscillation width at 200 Hz (Fig. 6). In the experiments, the welding speed for most cases was 3.0 m/min, whereas the welding speed oscillations with width less than 0.8 mm was increased to 3.5 m/min to prevent overheating from heat accumulation. At varying oscillation frequencies, the shortest crack was observed at 100 Hz, exactly where the longest crack was observed for the circular pattern. Moreover, the crack length increased beyond 100 Hz. (Fig. 7). The solidification crack propagated along the centerline for the self-restraint test with circular oscillation (Fig. 8(a)), whereas the crack propagated in a zigzag manner with infinite-shaped oscillation (Fig. 8(b)).

The molten pool behavior for the infinite-shaped beam oscillation was also observed with a high-speed camera. At 100 Hz, the shape of the pool noticeably transforms depending on the position of the laser keyhole (Fig. 9(a)). For nominal linear welding, the molten pool remained in a teardrop shape until the 100 Hz oscillation frequency. As shown in Fig. 2(c), the laser beam moves mostly transversely for some period, which was confirmed by the images taken between 0.006 s and 0.014 s, as shown in Fig. 9(a). As the

oscillation frequency increased, the molten pool exhibited a stable teardrop shape regardless of the laser keyhole location (Fig. 9(b)), similar to all the cases with the circular beam oscillation (Figs. 4(b) & (c)). The grain growth direction is determined by the movement of the solid-liquid interface [33-35]. At 100 Hz oscillation frequency, the pool generated a repetitively fluctuating morphology (Fig. 10(b)), as expected. The width of the equiaxed zone is inversely proportional to the bead width. With increasing oscillation frequency, the resulting fusion line straightened, resembling that in the linear weld. (Fig. 10 (c) and (d)). The equiaxed region at the center of fusion zone widened with the oscillation frequency as the temperature gradient was reduced.

The oscillating morphology of the sample under an oscillating frequency at 100 Hz resulted from the fluctuation of the grain growth rates (R) during solidification. In beam oscillation welding, the local solid-liquid interface movement, which determines the microstructure at the fusion zone, should be distinguished from the welding speed [29]. The shape of the molten pool is strongly influenced by the laser beam path. Both the laser beam path with the located keyhole and the outline of the molten pool were illustrated in Fig. 11. The time values in the images of the molten pool in Fig. 9(a) were chronologically labeled as t_1 to t_6, respectively. Furthermore, L represents the displacement of the solid-liquid interface after 0.004 s. The path was asymmetrical and involved an overlap of the translation motion of the scanner

and the beam scanning motion. From t_1 to t_3, the solid-liquid interface moved slowly along the welding direction. This could lead to a narrow equiaxed or columnar dendritic microstructure. However, from t4 to t6, the local grain growth rate at the center of the fusion zone rapidly increased, resulting in the dramatic reduction of the molten pool. Consequently, the local growth rate was significantly higher than the welding speed, and a wide equiaxed microstructure was generated. The path of the beam periodically overlapped, hence the equiaxed region was periodically distributed.

All the self-restraint test specimens exhibited dendritic and eutectic structures on the fracture surface. Smooth crack surfaces were evident, indicating that a thin liquid layer was present during hot cracking. On the fracture surface of the specimen at 100 Hz with an infinite-shaped beam pattern, the equiaxed and columnar regions alternated periodically (Fig. 12). Consequently, the solidification crack susceptibility in oscillating laser beam welding was strongly influenced by the distribution of the equiaxed zone along the centerline. Furthermore, a nonuniform equiaxed zone was preferred, whereas a wide and linear equiaxed zone should be avoided, in accordance with a previous study using low-frequency beam oscillation [31].

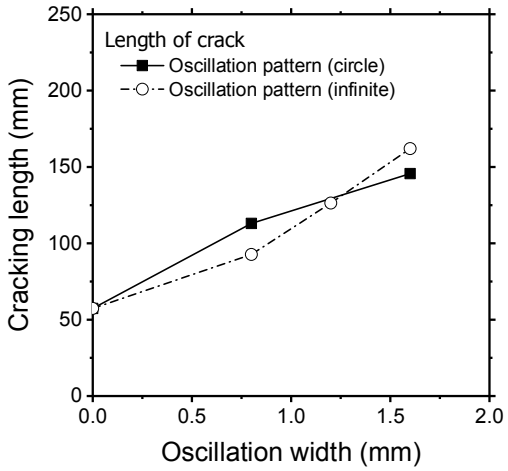

Figure 3.2.6 Measured length of the crack from different laser beam scanning patterns and oscillation widths. Specimens were fabricated under 900-W laser power at 200 Hz and 3 m/min welding speed.

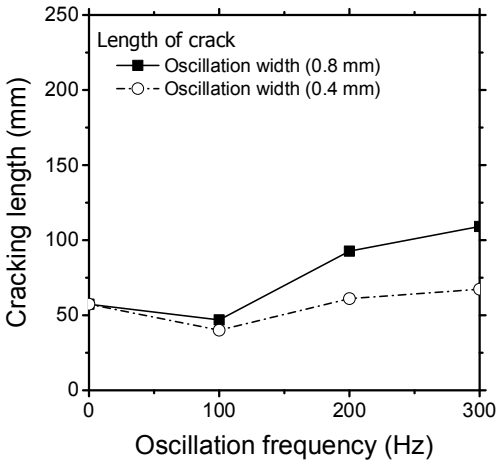

Figure 3.2.7 Measured length of the crack for different oscillation widths at varying frequencies. The specimen was prepared with an infinite-shaped pattern and laser power of 900 W at the welding speed of 3.5 m/min.

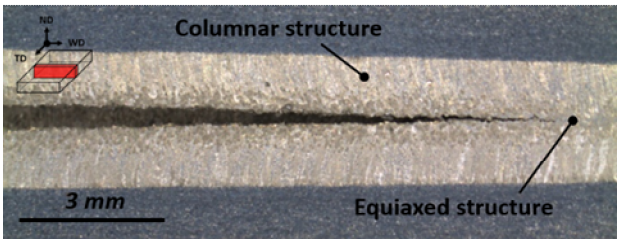

(a)

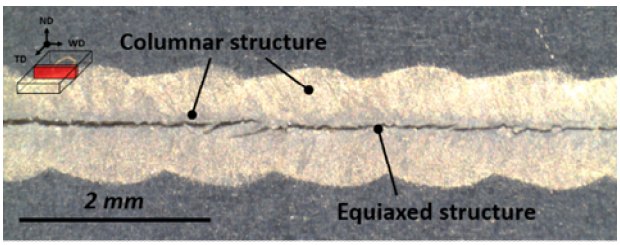

(b)

Figure 3.2.8 Bead appearance view from the normal direction depending on the welding condition (a). Circular scanning pattern with 900 W laser power and 1.6 mm oscillation width at 3 m/min welding speed and 100 Hz oscillation frequency; and (b) infinite-shaped scanning pattern 900 W laser power and 0.4 mm oscillation width at 100 Hz and 3 m/min welding speed.

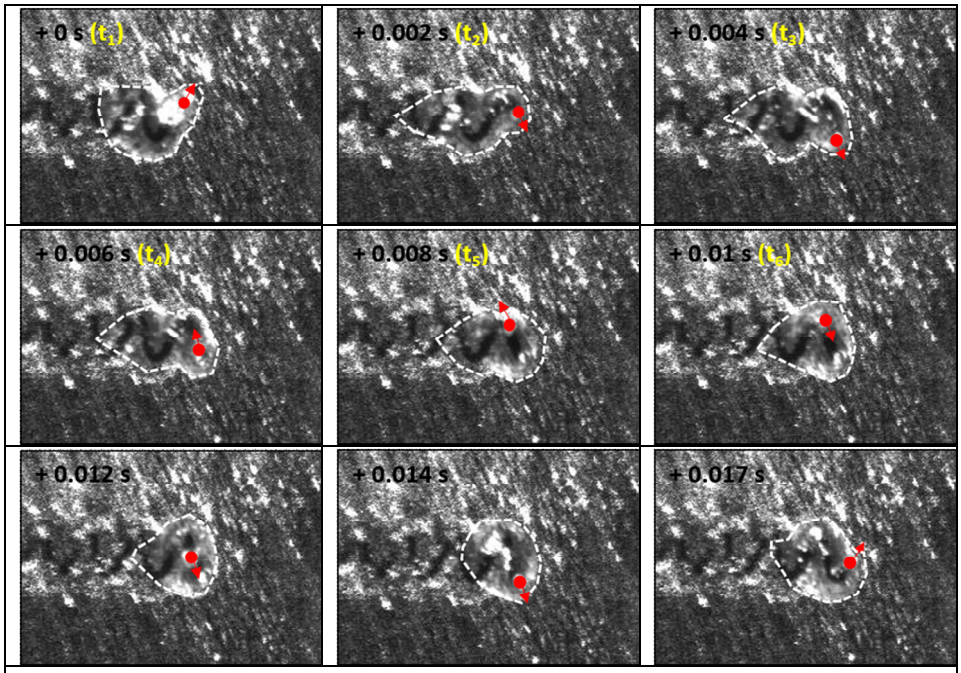

(a) 100 Hz, infinite-shaped pattern oscillation

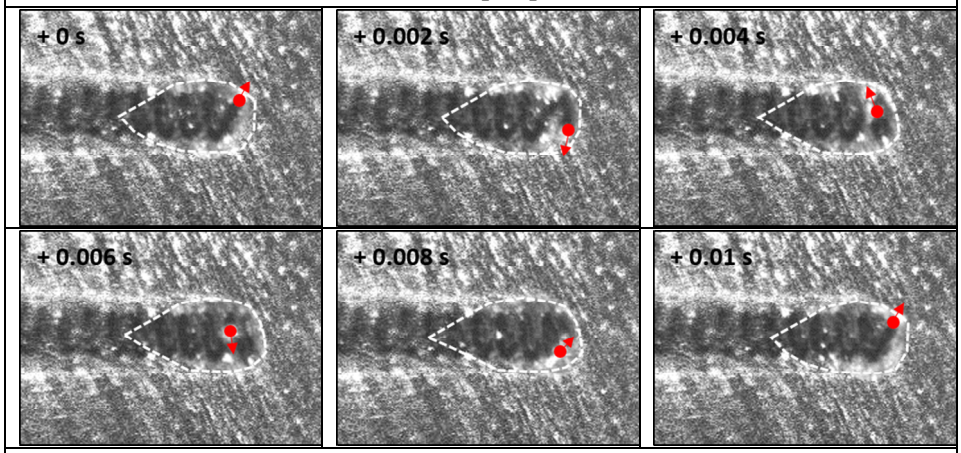

(b) 200 Hz, infinite-shaped pattern oscillation

Figure 3.2.9 High-speed camera images of the molten pool under laser beam

oscillation with an infinite-shaped pattern during a single oscillation. The oscillating laser beam welding was performed with 900 W laser power at 3.5 m/min. The oscillation width was fixed at 0.8 mm, while the frequency varied: (a) 100 and (b) 200 Hz.

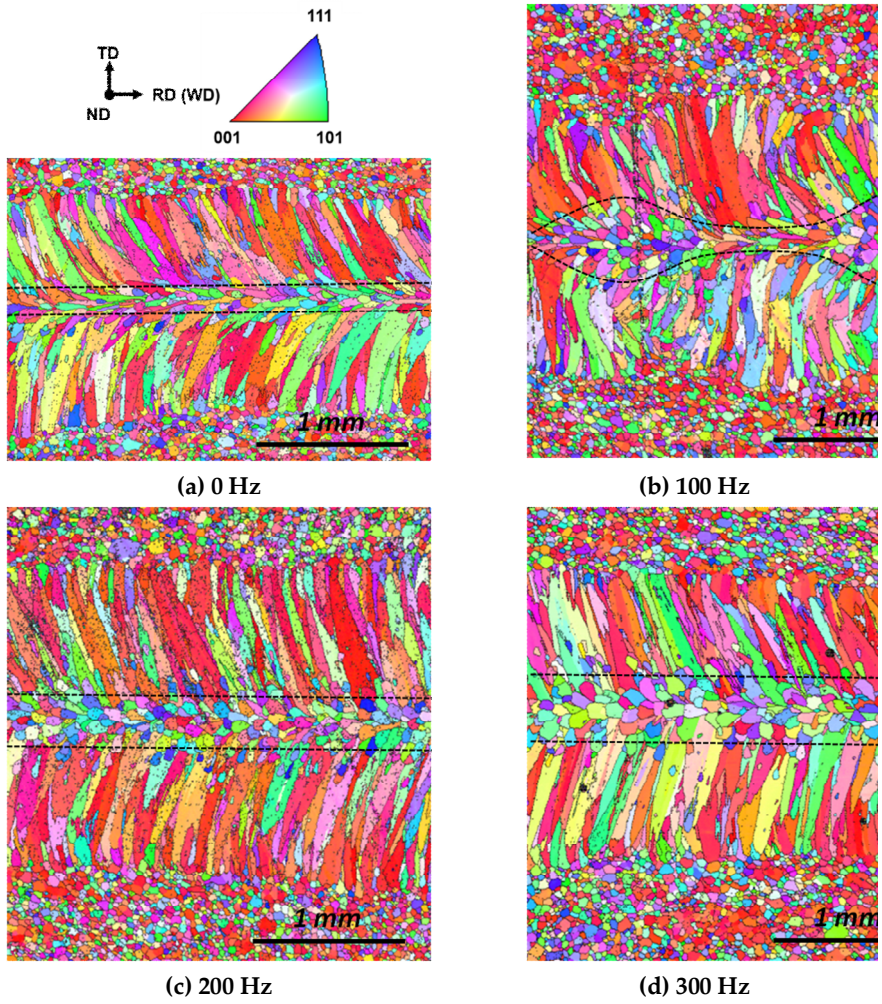

Figure 3.2.10 EBSD analysis with varying oscillation frequencies. Welding was performed with infinite-shaped beam pattern under 900 W laser power at 3.5 m/min welding speed. The oscillation width was fixed at 0.8 mm, while the frequency was varied at (a) 0 Hz, (b) 100 Hz, (c) 200 Hz, and (d) 300 Hz.

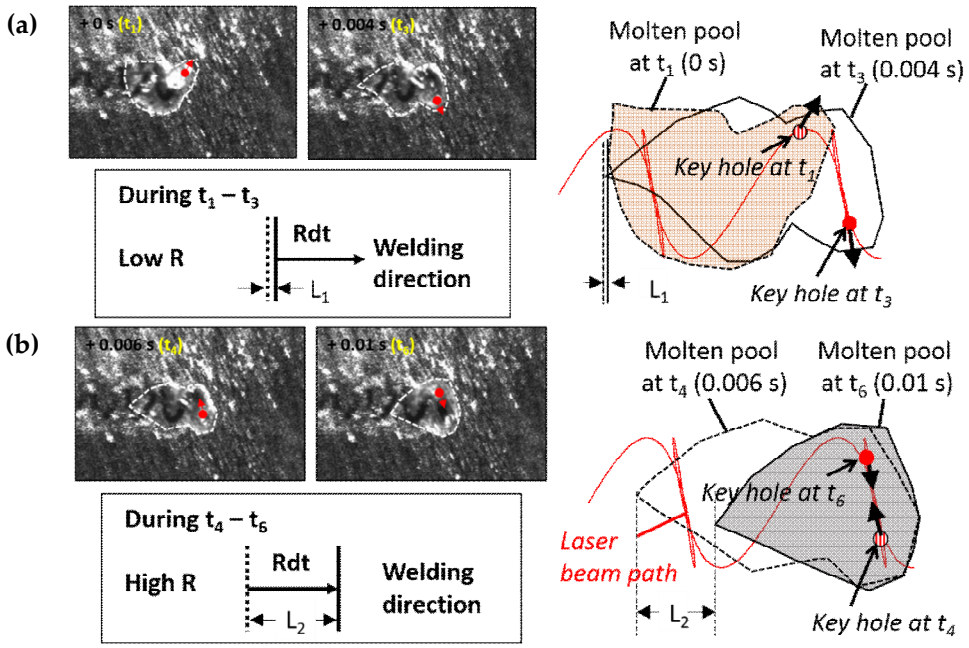

Figure 3.2.11 Schematic diagram of the molten pool movement, where R represents the local solidification rate, W.D is the welding direction along the x-axis, and Rdt indicates the solid-liquid interface displacement over a time interval.

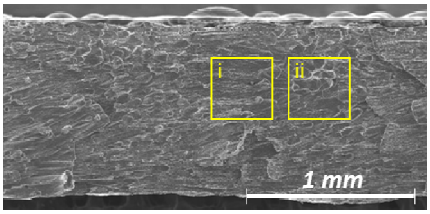

(a)

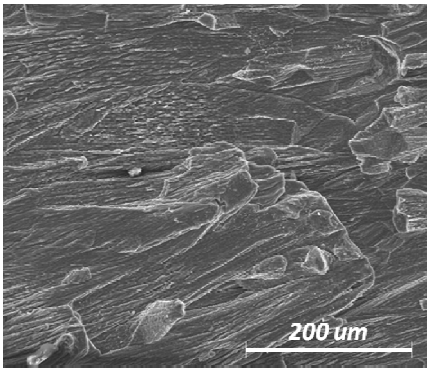

(b)

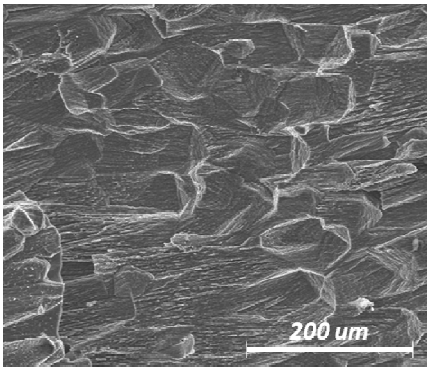

(c)

Figure 3.2.12 FESEM images of the specimens treated with oscillating laser beams at 100 Hz with the infinite-shaped pattern. (a) Fracture surface 1 mm from the start point; (b) high-magnification image of the yellow box region (i) in Fig. 12(a); and (c) high-magnification image of the yellow box region (ii) in Fig. 12(a).

3.2.5 Conlusions

Hot cracking susceptibility during laser welding with the beam oscillation of the automotive aluminum alloy, Al 6014, was evaluated using a self-restraint test. High-speed beam scanning and high laser beam density were implemented by galvanometers and single mode laser, respectively. In most cases, the keyhole moves with the molten pool at a very high speed and the boundary of the pool quasi-steadily transformed with the welding speed. Compared with linear welding, laser welding with beam oscillation resulted in a larger molten pool, and therefore increased cracking susceptibility, because the temperature gradient in the solidification region decreased, widening the equiaxed zone at the center of the fusion zone. However, a longitudinally oscillating bead shape was observed for an infinite-shaped scanning pattern at 100 Hz and 3.5 m/min welding speed. This originated from the sinuous movement of the laser beam along the longitudinal direction. The width of the equiaxed zone at the center of the fusion zone was also fluctuating. Consequently, crack propagation was hindered by this solidification morphology.

3.2.6 References

[1] Nakata, K., F. Matsuda, "Ductility characteristics of commercial aluminium alloys between liquidus and solidus temperatures during welding and evaluation of weld solidification cracking susceptibility", Welding international 9(9) 706-716 (1995).

[2] Eskin, D., L. Katgerman, "Mechanical properties in the semi-solid state and hot tearing of aluminium alloys", Progress in Materials Science 49(5) 629-711 (2004).

[3] Cross, C., On the origin of weld solidification cracking, Hot cracking phenomena in welds, Springer2005, pp. 3-18.

[4] Zhao, H., D. White, T. DebRoy, "Current issues and problems in laser welding of automotive aluminium alloys", International Materials Reviews 44(6) 238-266 (1999).

[5] Dowd, J., "Weld cracking of aluminum alloys", Welding Journal 31(10) 448s-456s (1952).

[6] Dudas, J., C. FR, "Preventing weld cracks in high strength aluminum alloys", Welding journal 45(6) 241s-249s (1966).

[7] Savage, W., E. Nippes, J. Varsik, "Hot-Cracking Susceptibility of 3004 Aluminum", Welding Journal 58(2) (1979).

[8] Matsuda, F., K. Nakata, "A New Test Specimen for Self-Restraint Solidification Crack Susceptibility Test of Electron-Beam Welding Bead:

Fan-Shaped Cracking Test ", Transactions of JWRI 11 87-94 (1982).

[9] Cicală, E., G. Duffet, H. Andrzejewski, D. Grevey, S. Ignat, "Hot cracking in Al–Mg–Si alloy laser welding–operating parameters and their effects", Materials Science and Engineering: A 395(1) 1-9 (2005).

[10] Ploshikhin, V., A. Prikhodovsky, A. Ilin, M. Makhutin, C. Heimerdinger, F. Palm, "Influence of the weld metal chemical composition on the solidification cracking susceptibility of AA6056-T4 alloy", Welding in the World 50(11-12) 46-50 (2006).

[11] Ahn, Y. N., C. H. Kim, "Evaluation of Crack Sensitivity and Gap Bridging Ability during Laser Butt Welding of Aluminum 5J32 and 6K21 Alloys", Materials Science Forum 695 247-250 (2011).

[12] Langrieger, H., F. Krafft, M. Mensinger, F. Oefele, "Thermomechanical analysis of the formation of hot cracks in remote laser welded aluminium fillet welds", Journal of Laser Applications 28(2) 022414 (2016).

[13] Kuryntsev, S. V., A. K. Gilmutdinov, "The effect of laser beam wobbling mode in welding process for structural steels", The International Journal of Advanced Manufacturing Technology 81(9-12) 1683-1691 (2015).

[14] Hao, K., G. Li, M. Gao, X. Zeng, "Weld formation mechanism of fiber laser oscillating welding of austenitic stainless steel", Journal of Materials Processing Technology 225 77-83 (2015).

[15] Schmitt, F., B. Mehlmann, J. Gedicke, A. Olowinsky, A. Gillner, R. Poprawe, "Laser beam micro welding with high brilliant fiber lasers", J

Laser Micro/Nanoeng 5(3) 197-203 (2010).

[16] Sommer, M., J.-P. Weberpals, S. Müller, P. Berger, T. Graf, "Advantages of laser beam oscillation for remote welding of aluminum closely above the deep-penetration welding threshold", Journal of Laser Applications 29(1) 012001 (2017).

[17] Albert, F., P. Marben, T. Graham, "Remote Laser Welding of Steel and Aluminum Alloys", Laser Technik Journal 14(1) 32-35 (2017).

[18] Barbieri, G., F. Cognini, M. Moncada, A. Rinaldi, G. Lapi, "Welding of automotive aluminum alloys by laser wobbling processing", Materials Science Forum 879 1057-1062 (2017).

[19] Fetzer, F., M. Jarwitz, P. Stritt, R. Weber, T. Graf, "Fine-tuned Remote Laser Welding of Aluminum to Copper with Local Beam Oscillation", Physics Procedia 83 455-462 (2016).

[20] Wei, H., J. Elmer, T. DebRoy, "Crystal growth during keyhole mode laser welding", Acta Materialia 133 10-20 (2017).

[21] Wang, L., M. Gao, C. Zhang, X. Zeng, "Effect of beam oscillating pattern on weld characterization of laser welding of AA6061-T6 aluminum alloy", Materials & Design 108 707-717 (2016).

[22] Kraetzsch, M., J. Standfuss, A. Klotzbach, J. Kaspar, B. Brenner, E. Beyer, "Laser beam welding with high-frequency beam oscillation: welding of dissimilar materials with brilliant fiber lasers", Physics Procedia 12 142-149 (2011).

[23] Dittrich, D., A. Jahn, J. Standfuss, E. Beyer, "Laser beam welding of atmosphere aluminum die cast material using high frequency beam oscillation and brilliant beam sources", Journal of Laser Applications 29(2) 022425 (2017).

[24] Kou, S., Y. Le, "Grain structure and solidification cracking in oscillated arc welds of 5052 aluminum alloy", Metallurgical Transactions A 16(7) 1345-1352 (1985).

[25] Gollnow, C., A. Griesche, J. Weidemann, T. Kannengiesser, "Influence of external loads on a characteristic angle between grains and solidus line as an indicator for hot cracking susceptibility during GTA welding", Journal of Materials Processing Technology 239(Supplement C) 172-177 (2017).

[26] Shinozaki, K., P. Wen, M. Yamamoto, K. Kadoi, Y. Kohno, T. Komori, "Effect of grain size on solidification cracking susceptibility of type 347 stainless steel during laser welding", (2010).

[27] Tang, Z., F. Vollertsen, "Influence of grain refinement on hot cracking in laser welding of aluminum", Welding in the World 58(3) 355-366 (2014).

[28] von Witzendorff, P., S. Kaierle, O. Suttmann, L. Overmeyer, "Using pulse shaping to control temporal strain development and solidification cracking in pulsed laser welding of 6082 aluminum alloys", J. Mater. Process. Technol. 225 162-169 (2015).

[29] Von Witzendorff, P., S. Kaierle, O. Suttmann, L. Overmeyer, "In situ

observation of solidification conditions in pulsed laser welding of AL6082 aluminum alloys to evaluate their impact on hot cracking susceptibility", Metallurgical and Materials Transactions A 46(4) 1678-1688 (2015).

[30] Choi, K.-D., Y.-N. Ahn, C. Kim, "Weld strength improvement for Al alloy by using laser weaving method", Journal of Laser Applications 22(3) 116-119 (2010).

[31] Kim, C., M. Kang, N. Kang, "Solidification crack and morphology for laser weave welding of Al 5J32 alloy", Science and Technology of Welding and Joining 18(1) 57-61 (2013).

[32] Dan, W., S. Shuntaro, K. Kota, S. Kenji, Y. Motomichi, "Investigation of Evaluation Method for Hot Cracking Susceptibility of 310S Stainless Steel during Laser Welding using Trans-Varestraint Test", Quarterly Journal of the Japan Welding Society 33(2) 39s-43s (2015).

[33] Kou, S., Welding metallurgy, Second ed., John Wiley & Sons, New York, USA, 2002.

[34] David, S., J. Vitek, "Correlation between solidification parameters and weld microstructures", International Materials Reviews 34(1) 213-245 (1989).

[35] Wei, H., J. Elmer, T. DebRoy, "Three-dimensional modeling of grain structure evolution during welding of an aluminum alloy", Acta Materialia 126 413-425 (2017).

Chapter 4

Analysis of stress fields subjected to the laser oscillation welding and its effect on hot cracking susceptibility.

4.1 Introduction:

By the development and commercialization of electric cars and hybrid cars, the application of aluminum to car body is gradually expanding. Welding is the main joining process of an automotive steel structure, and resistance spot welding, gas metal arc welding, and laser welding are the most frequently used welding processes for automotive steel sheets. In the laser welding for aluminum alloy, such as 2XXX [1], 6XXX [2-4] and 7XXX [5], has a limitation due to the weld defect as solidification crack. In order to control the chemical composition of weld metal, it is necessary to readjust the chemical composition of the aluminum base metal or to add auxiliary filler wire. Optimization of the weld composition using a filler metal is a conventional method used to prevent solidification cracking [6]. However, the application of filler metals has a limit to an actual process owing to the small heat source and inhomogeneity of the composition in the molten pool.

Solidification cracking has been evaluated for various fusion welding processes such as arc welding [7-9], electron beam welding [10], and laser beam welding [4,11-13]. By applying the laser welding, thermal distortion can be reduced results from a low heat input by using high-density energy. Recently, a beam oscillation method was suggested using galvanometric, which allowing the use of wide weld beads and controlling the thermal history of welds [14-16]. Therefore, attempts were tried to suppress the formation of solidification cracks during the laser welding by oscillating the laser beam and controlling the laser power with a pulse waveform. The effect of oscillation of heat source on the microstructural evolution [17], solidification crack susceptibility [13], and welding strength [18] has been investigated. Choi et al. [19] applied a low-frequency laser oscillation on the 6K21 Al alloy to improve its joint strength. Notably, oscillation of the heat source changed the shape of weld beads and solidification morphology obtained through columnar and equiaxed dendritic growth. However, the formation of hot cracking on fillet joint subjected laser beam oscillation is still an unknown field.

In order to obtain understanding of hot cracking behavior depending on penetration mode with lap fillet joint, we performed laser beam oscillation welding under various oscillation width and frequency. To evaluate the effect of oscillation parameter, the regression analysis was progressed using the shape of bead and length of the hot cracking.

4.2 Effects of laser oscillation parameter to the penetration mode

For the welding process, a Yb:YAG laser, YLS-3000 (IPG Photonics, Oxford, MA, USA), was applied. The laser beam was delivered through an optical fiber with a diameter of 100 m. The path was implemented by a single-axis translation system and two-axis beam scanner, D30 (IPG Photonics, Oxford, MA, USA), with a focal length of 250 mm (Fig. 1(a)). The laser beam was perpendicularly irradiated to the specimen and was focused on the upper surface of the workpiece with a beam diameter of 0.28 mm. Ar shielding gas was provided to the side during welding. To evaluate the hot cracking susceptibility for the lap joint welds under different welding conditions, a self-restraint test specimen was modified and fabricated as shown in Fig. 1 [10]. Laser welding initiated at the narrow edge and ended at the wide one. A laser beam was subjected to the edge of the upper plate. The base material was a 1 mm-thick Al 6014-T4 alloy. The chemical composition of the base material is shown in Table 1..

In this study, circular patterns were adopted and compared with general linear motion. To investigate the influence of penetration depth on hot crack susceptibility, the oscillation width and frequency were varied. During the laser welding, tensile and rotation stress field were generated near of fusion zone due to the thermal expansion (Fig. 2(a)). During the experiment, the

crack can be found at the center of the fusion zone as like in Fig. 2(b). Figure 3 shows the laser beam path for the circular beam patterns at different frequencies. The laser power and welding speed were fixed as 2300 W and 3 m/min, respectively. The details of the laser welding conditions are presented in Table 2. After welding, a non-destructive X-ray test was conducted to measure the hot cracking length using XSCAN-H160 (XAVIS, Seongnam, Gyeonggi, Korea). The surface of the samples was polished and etched by Keller's etchant. To characterize the effect of bead shape on cracking, the section of welds observed in two separate samples.

Table 4.1 Chemical compositions measured with ICP analyzer and mechanical properties of applied base material (wt. %)

Chemical compositions (wt. %)								
Si	Fe	Cu	Mn	Mg	Cr	Zn	Ti	Al
0.58	0.21	0.14	0.08	0.64	0.01	0.01	0.03	Bal.

Mechanical properties		
Tensile strength* (MPa)	Yield strength* (MPa)	Elongation at fracture* (%)
234	126	24

*: average of the results of three quasi-static tensile tests.

Table 1. Laser welding conditions

Laser power	2300 W
Welding speed	3 m/min
Oscillation width	0 ~ 1.6 mm
Oscillation frequency	0 ~ 400 Hz
Beam pattern	Circle
Shielding gas	Ar shielding
Focal position	0 mm
Offset	0 mm
Beam tilting angle	0°

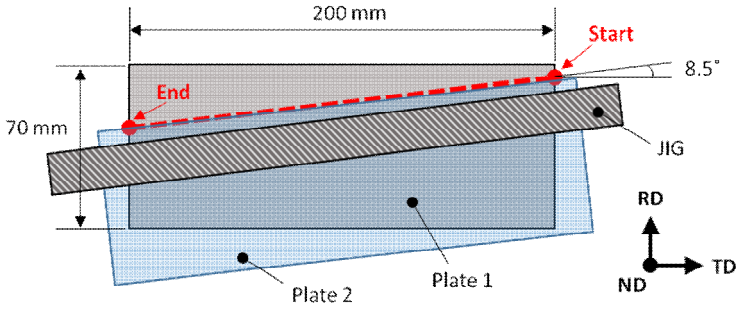

(b)

Figure 4.1 Schematic image of the laser overlapped specimen to evaluate hot cracking susceptibility.

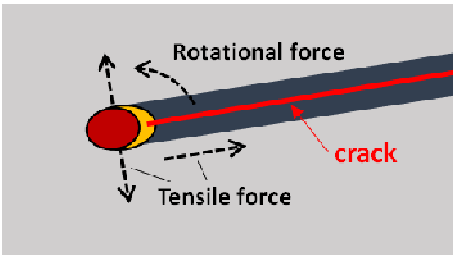

(a)

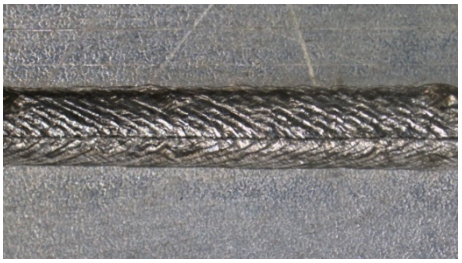

(b)

Figure 4.2 (a) Schematic images of active force during the laser welding, and (b) generated crack at the center of a lap fillet joint.

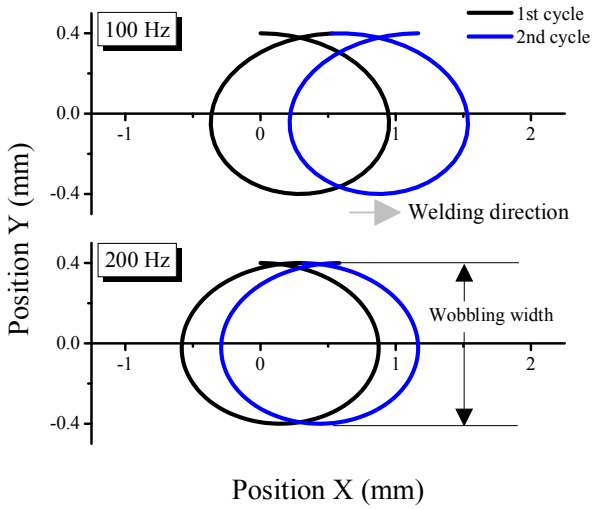

Figure 4.3 Laser oscillation beam patterns circularly at a welding speed of 3 m/min, oscillation width of 0.8 mm and oscillation frequency of (a) 100 Hz; (b) 200 Hz.

4.3 The Effects of the bead appearance subjected laser beam oscillation on hot cracking susceptibility

Oscillation width and frequency affected the bead appearance. The shape of the joint has an importance because it affects the stress distribution of the joint. When the laser beam oscillation was applied to the welds, joint bridging ability can be enhanced. The undercut was found near of the fusion line on the top plate when the oscillation was not applied or the width was narrow (Fig. (a) and (b)). By increasing of oscillation width, the edge near of the fusion line getting smooth. These phenomena had an advantage to the stress distribution. Also, the laser beam oscillation has a benefit for the welds seam tracking. However, the oscillation width was widened over the critical oscillation width, the joint was not be melted due to the lack of fusion result from insufficient heat input.

Figure 5 shows the macro-section images of the specimen according to the oscillation frequency. These were fabricated under the same laser power, welding speed, and the oscillation width was fixed at 0.8 mm. To evaluate the effect of bead appearance, factors led from section images were defined and named as bead width of interface is a_1, bead width at top surface is a_2, thickness of throat is a_3, bead width at bottom surface is a_4, penetration depth is a_5, and molten area is s_1, respectively as shown in Figure 5 (a). Both oscillation width and frequency affect the heat input subjected to the specimen,

which changes the shape of the fusion zone. Compared to linear welding (Fig. 5(a)), a shallow the fusion zone was produced by the oscillating laser beams. With an oscillation frequency of 100 Hz, the full penetration welds were obtained at 0.8 mm mm oscillation frequency (Fig. 5(b)). Beyond this frequency (Fig. 5(c) and (d)), the penetration depth (a_5) became shallow and the bead width at the bottom surface was decreasing. The details of the bead shape factors according to the laser beam oscillation parameters were presented in Fig. 6. From the results, it can be confirmed that the shape factor a_3, a_5, and s_1 had a high variation depending on oscillation frequency.

The hot cracking lengths evaluated by non-destructive X-ray test and present in Fig. 7. When the laser beam oscillation was applied, shorter cracks were observed at higher oscillation widths. At oscillation frequency of 100 Hz, the length of the crack increased with the oscillation width. However, the shape factor of a_1 and a_2 varied almost uniformly independent of the oscillation width and frequency. By using the regression analysis (Table 3(a)) between the shape factor and length of crack, it was confirmed that bead width at bottom surface (a_3) had a high correlation compare with the others.

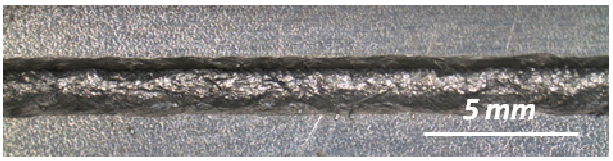

(a)

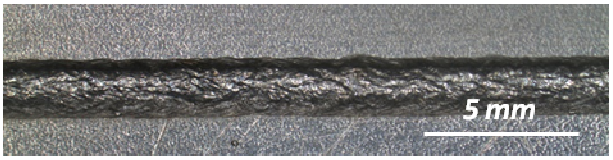

(b)

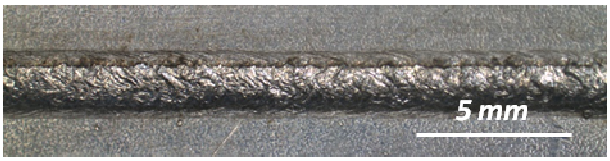

(c)

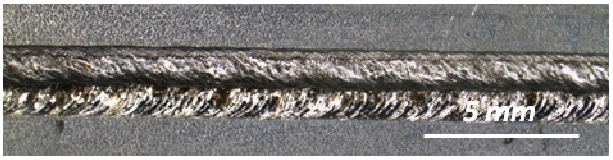

(d)

Figure 4.4 bead appearance of the specimen prepared using an oscillation frequency of 200 Hz and oscillation width of (a) 0.2 mm; (b) 0.4 mm; (c) 0.8 mm; and (d) 1.6 mm.

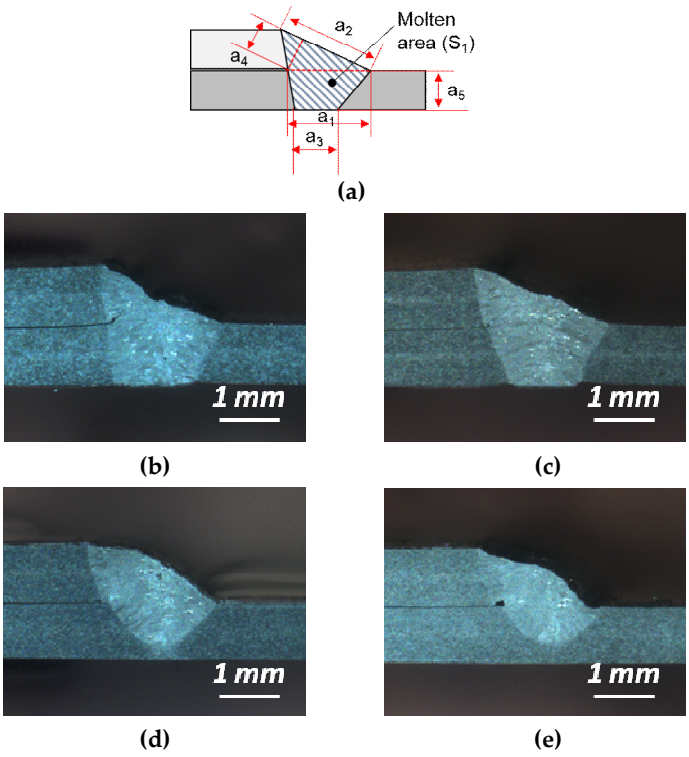

Figure 4.5 (a) Definition of shape factor on section image, and macro-section images (b)-(e) according to the oscillation width. The welding was performed by circular beam pattern under 2300 W laser power, 3 m/min welding speed. The oscillation width was 0.8 mm. (b) 0 Hz; (c) 100 Hz; (d) 200 Hz; (e) 300 Hz.

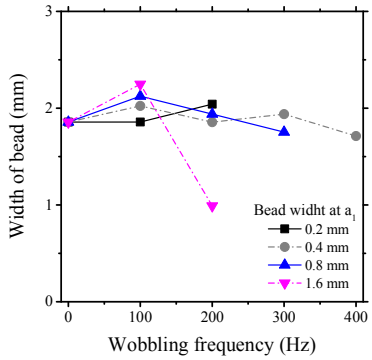
Width of bead (mm)
Wobbling frequency (Hz)
Bead widht at a1
0.2 mm
0.4 mm
0.8 mm
1.6 mm

(a)

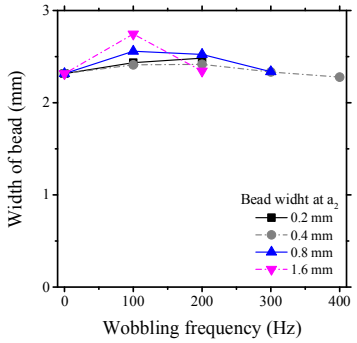
Width of bead (mm)
Wobbling frequency (Hz)
Bead widht at a2
0.2 mm
0.4 mm
0.8 mm
1.6 mm

(b)

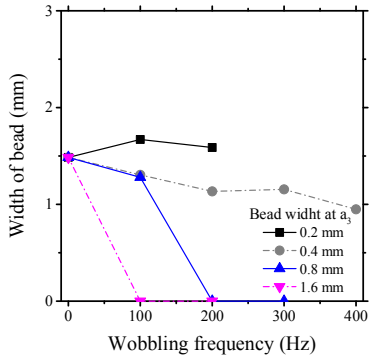
Width of bead (mm)
Wobbling frequency (Hz)
Bead widht at a3
0.2 mm
0.4 mm
0.8 mm
1.6 mm

(c)

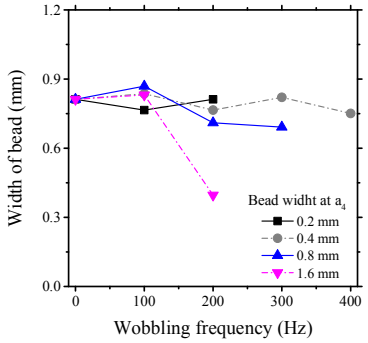
Width of bead (mm)
Wobbling frequency (Hz)
Bead widht at a4
0.2 mm
0.4 mm
0.8 mm
1.6 mm

(d)

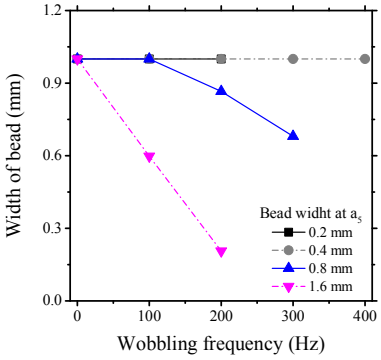
Width of bead (mm)
Wobbling frequency (Hz)
Bead widht at a5
0.2 mm
0.4 mm
0.8 mm
1.6 mm

(e)

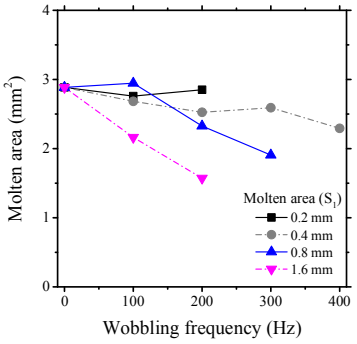
Molten area (mm2)
Wobbling frequency (Hz)
Molten area (S1)
0.2 mm
0.4 mm
0.8 mm
1.6 mm

(f)

Figure 4.6 Analysis of bead appearances according to the oscillation width and frequency. (a) bead width at interfacial (a_1); (b) bead width at top surface (a_2); (c) thickness of throat (a_3); (d) bead width at bottom surface (a_4); (e) depth of the welds (a_5); (f): molten area (s_1)

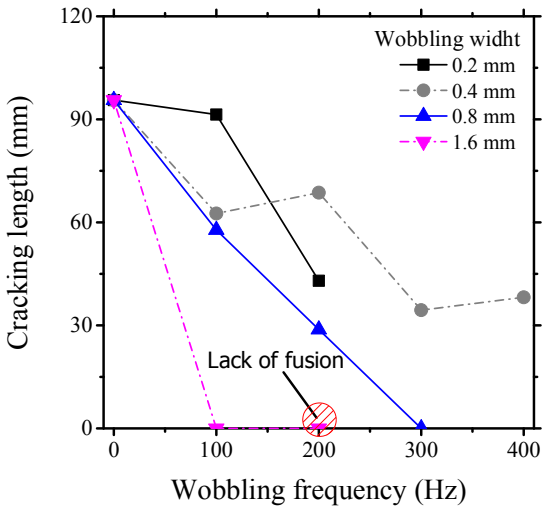

(a)

Figure 4.7 Measured crack lengths depending on oscillation width and frequency, which was evaluated by non-destructive X-ray test.

Table 3. Results of regression analysis between the shape factors and length of crack.

(a) Pearson correlation analysis

Measuring point	Interface bead width (a_1)	Top bead width (a_2)	Bottom bead width (a_3)	Throat thickness (a_4)	Depth of the welds (a_5)	Molten area (s_1)
Unit	mm	mm	mm	mm	mm	mm^2
Pearson correlation	0.272	-0.212	0.861**	0.491	0.74**	0.818**
Significantly change	0.393	0.509	0	0.105	0.006	0.001

(b) Stepwise regression analysis of a_3

Model	R square	F	Degree of freedom	Estimation	β_1	β_2
Linear regression	0.741	28.548	10	6.215	42.217	
Polynomial regression of order 2	0.745	13.147	9	7.074	29.057	8.956

4.4 Conlusions

In order to obtain the understanding of hot cracking for the aluminum alloy with lap fillet joint, modified self-restraint test was performed. High-speed beam scanning and high laser beam density were implemented by galvanometers with a multi-mode laser. The penetration depth was varied according to the oscillation width and frequency, and the length of cracking was reduced as decreasing of the width of back bead (a_3). Compared with full penetration weldments, partial penetration weldments resulted in a shallow penetration depth and less susceptible to the cracking. From the results, it was verified that hot cracking can be suppressed by the change of penetration mode.

4.6 References

1. Sheikhi, M.; Ghaini, F.M.; Assadi, H. Prediction of solidification cracking in pulsed laser welding of 2024 aluminum alloy. Acta Materialia 2015, 82, 491-502.
2. Von Witzendorff, P.; Kaierle, S.; Suttmann, O.; Overmeyer, L. In situ observation of solidification conditions in pulsed laser welding of Al6082 aluminum alloys to evaluate their impact on hot cracking susceptibility. Metallurgical and Materials Transactions A 2015, 46, 1678-1688.
3. Wei, H.; Chen, J.; Wang, H.-P.; Carlson, B.E. Thermomechanical numerical analysis of hot cracking during laser welding of 6xxx aluminum alloys. Journal of Laser Applications 2016, 28, 022405.
4. Ploshikhin, V.; Prikhodovsky, A.; Ilin, A.; Makhutin, M.; Heimerdinger, C.; Palm, F. Influence of the weld metal chemical composition on the solidification cracking susceptibility of aa6056-t4 alloy. Welding in the World 2006, 50, 46-50.
5. Hu, B.; Richardson, I. Mechanism and possible solution for transverse solidification cracking in laser welding of high strength aluminium alloys. Materials Science and Engineering: A 2006, 429, 287-294.
6. Hiroto, Y.; Masahiro, Y.; Kazuyuki, T. The study of prevention of solidification cracking in laser weld metal of Al-Mg-Si alloy. Journal of

japan welding society 2000, 18, 422-430.

7. Dowd, J. Weld cracking of aluminum alloys. Welding Journal 1952, 31, 448s-456s.
8. Dudas, J.; FR, C. Preventing weld cracks in high strength aluminum alloys. Welding journal 1966, 45, 241s-249s.
9. Savage, W.; Nippes, E.; Varsik, J. Hot-cracking susceptibility of 3004 aluminum. Welding Journal 1979, 58.
10. Matsuda, F.; Nakata, K. A new test specimen for self-restraint solidification crack susceptibility test of electron-beam welding bead: Fan-shaped cracking test Transactions of JWRI 1982, 11, 87-94.
11. Cicală, E.; Duffet, G.; Andrzejewski, H.; Grevey, D.; Ignat, S. Hot cracking in al–mg–si alloy laser welding–operating parameters and their effects. Materials Science and Engineering: A 2005, 395, 1-9.
12. Ahn, Y.N.; Kim, C.H. Evaluation of crack sensitivity and gap bridging ability during laser butt welding of aluminum 5J32 and 6K21 alloys. Materials Science Forum 2011, 695, 247-250.
13. Langrieger, H.; Krafft, F.; Mensinger, M.; Oefele, F. Thermomechanical analysis of the formation of hot cracks in remote laser welded aluminium fillet welds. Journal of Laser Applications 2016, 28, 022414.
14. Kraetzsch, M.; Standfuss, J.; Klotzbach, A.; Kaspar, J.; Brenner, B.; Beyer, E. Laser beam welding with high-frequency beam oscillation: Welding of dissimilar materials with brilliant fiber lasers. Physics

Procedia 2011, 12, 142-149.

15. Kuryntsev, S.V.; Gilmutdinov, A.K. The effect of laser beam wobbling mode in welding process for structural steels. The International Journal of Advanced Manufacturing Technology 2015, 81, 1683-1691.
16. Schmitt, F.; Mehlmann, B.; Gedicke, J.; Olowinsky, A.; Gillner, A.; Poprawe, R. Laser beam micro welding with high brilliant fiber lasers. J Laser Micro/Nanoeng 2010, 5, 197-203.
17. Wang, L.; Gao, M.; Zhang, C.; Zeng, X. Effect of beam oscillating pattern on weld characterization of laser welding of AA6061-T6 aluminum alloy. Materials & Design 2016, 108, 707-717.
18. Kim, B.-H.; Kang, N.-H.; Park, Y.-H.; Ahn, Y.-N.; Kim, C.-H.; Kim, J.-H. A study to improve weld strength of al 6K21-T4 alloy by using laser weaving method. Journal of Welding and Joining 2009, 27, 49-53.
19. Choi, K.-D.; Ahn, Y.-N.; Kim, C. Weld strength improvement for al alloy by using laser weaving method. Journal of Laser Applications 2010, 22, 116-119.

Chapter 5

Total conclusion

The laser was first introduced into the microelectronics industry in the late 1960s for sealing electronic packages and thin-wire connections. At present, laser welding is a proven joining technique in the automotive, metals (parts supply), shipyard, microelectronics, packaging, and aerospace industries. A laser has a high-power density heat source. Therefore, 'laser welding' is recognized as an advanced process to join materials with a laser beam of high-power, high-energy density. Laser welding promising joining technology with high quality, high precision, high performance, high speed, good flexibility and low distortion. Consequently, application of laser welding is increasing with the development of novel laser apparatuses and joining processes.

On the other hand, the development and commercialization of electric cars and hybrid cars, the application of aluminum to car body is gradually expanding. However, solidification cracking is frequently observed in aluminum welds. The low ductility of a semi-solid in the mushy zone and the high solidification shrinkage of aluminum alloys both increase hot cracking susceptibility. Solidification cracking is initiated by complex interactions between metallurgical and mechanical factors, not by one factor. During laser

welding, this can be diminished by improving chemical composition, refining solidification structure, optimizing laser pulsing parameters, and/or reducing thermal strains. This is very important that deep understanding for the affecting factors to suppress the hot cracking propagation during laser welding, Since the changing of chemical composition by adding a filler wire is not practical for the laser welding, the effects of thermal cycle and residual stress of the welds have to be considered more seriously.

Various laser welding process was selected to change the thermal cycle. Also, these effects on microstructural and mechanical properties were investigated, too. Therefore, the complex physics during laser welding depending on penetration depth, the finite element method based on the thermal conduction was conducted for the simulation.

Microstructural evolution highly related with thermal cycle resulted from temperature gradient and solidification rate. According to the welding parameters, the width of the equiaxed region was varied and the direction of grain growth has fluctuated. Firstly, the microstructural change in the laser welds of Al 6014 alloy is analyzed. High-quality, defect-free welds are successfully produced by ARM laser which can be changed the beam profile freely. An equiaxed structure was formed at the center of the welds, and the equiaxed region compared with fusion zone width was increased as increasing of welding speed. Hot cracking susceptibility was decreased as increasing of equiaxed fraction per unit area. It means that the microstructure formation of

the welds affects the hot cracking propagation.

Molten pool size and shape directly influence hot cracking susceptibility. To evaluate the influence of oscillation parameters, laser beam oscillation welding was performed with different beam patterns, widths, and frequencies. The behavior of hot cracking propagation was analyzed by a high-speed camera and electron backscatter diffraction. The behavior of crack propagation was observed to be highly correlated with the microstructural evolution of the fusion zone. For an oscillation with an infinity-shaped scanning pattern at 100 Hz and 3.5 m/min welding speed, the bead width, solidification microstructure, and the width of the equiaxed zone at the center of fusion were fluctuating. Furthermore, the equiaxed and columnar regions alternated periodically, which could reduce solidification cracking susceptibility. This originated from the sinuous movement of the laser beam along the longitudinal direction. Consequently, crack propagation was hindered by the formation of solidification morphology.

The crack propagation was highly related with the bead appearance. When penetration mode changed from full to partial penetration, length of hot cracking was reduced. To analyze the influence of penetration mode, bead shape factor was analyzed. From the results, it is confirmed that length of crack resulted from the variation of penetration mode of the welds affected by the shape factors of welds.

From this study, the effects of thermal cycle and shape on hot cracking

susceptibility, which has not been clear up to now, is described well. Experimental results lead to a clearer understanding about hot cracking propagation during laser welding of 6XXX series of aluminum alloy, sensitive to hot cracking. These results can be used beneficially to arrange an alternative methodology to avoid hot cracking.

국문 초록

레이저 용접법은 전자산업에서 전자기 패키지를 연결하기 위한 미세 와이어를 연결하기 위한 방법으로 1960년에 소개된 기술이다. 현재는 기술개발과 더불어 자동차, 철강회사 (판재의 연속공급을 위한 방안), 조선, 전자, 패키징, 심지어 우주산업에까지 널리 적용되고 있다. 레이저 용접은 고밀도의 집적에너지를 가지고 용접을 수행하는 공정법으로써, 적은 입열을 사용하여 공정이 진행되기 때문에 여타의 용융공정에 비하여 변형이 적게 발생될 뿐만 아니라 우수한 용접부 품질과 정확도, 빠른 공정속도로 인한 높은 생산성, 다양한 공정 적용성 등을 만족시킬 수 있다.

최근 전기차 하이브리드차의 개발과 더불어 알루미늄의 차체 적용이 증가하고 있다. 이에 따라, 레이저의 차체 적용 가능성 또한 증가하고 있다. 고온균열에 민감한 알루미늄의 경우, 저입열 공정이 필수적으로 요구될 것으로 예측되며 그 일환의 하나로 레이저 용접공정이 제안되고 있다. 그러나 알루미늄의 높은 열전도도와 열팽창률으로 인해 레이저 용접 중에도 고온균열이 빈번히 발생된다고 알려져 있으며, 본 실험결과에서도 균열의 형성이 확인되었다. 이러한 현상은 mush zone이라고 알려져 있는 반고체

상태의 영역에서의 연성저하에 의해 나타난다고 보고된 바 있으며, 알루미늄, 스테인레스 스틸, 니켈 합금 등 몇몇의 합금에 대하여 주조 또는 용접을 할 때 빈번히 관찰된다.

많은 연구자에 의하여 발생 및 전파 매커니즘이 연구되어지고 있으나 현재까지도 원인이 명확히 규명되지 못하였다. 이것은 고온균열의 발생 및 전파가 단독요인에 의한 것이 아니라 조직적, 기계적 요인이 복합적으로 작용되었을 때 진행되기 때문이다.

고온균열의 발생 및 전파를 억제하기 위하여 합금첨가를 통한 응고조직의 미세화, 레이저 출력을 펄스파형으로 공급하는 방법 등이 제안되어 있다. 또한 비드의 형상을 변화시키거나 레이저 용접 전 후 추가 입열을 공급하여 열이력을 바꾸는 방법 등도 시도되고 있다. 보편적으로 Si이 다량 포함되어 있는 용가재를 추가공급하여 용융부의 조성을 제어하는 방안을 적용하고 있으나, 용가재를 추가 사용하여야 하기 때문에 생산단가가 올라갈 뿐만 아니라, 레이저 빔을 추적하는 기술이 추가적으로 요구되며 공정자유도가 제한되어 생산성을 저해하는 요인으로 작용할 수 있다. 때문에 조성을 제어하는 방법이 아닌 앞서 언급한 레이저 열원 공급방법 변화 및 비드의 형상 및 공정 변화를 통한 연구가 현장적용성이 높다고 볼 수 있다.

본 연구에서는 열이력을 변화시키기 위하여 레이저 용접공정 중의 변화를 도모하였으며, 이것이 조직적/기계적 특성에 미치는 영향을 고찰하였다.

실험결과, 조직의 형성은 열이력과 높은 상관관계를 가지고 있음을 알 수 있었다. 용접변수가 열이력에 영향을 미치기 때문에 국부적 온도구배와 응고속도는 변수에 따라 변화하게 된다. 때문에 용접조건에 따라 용접부 중심에 형성되는 등축정 조직의 크기 및 형성 구간은 변화한다. 뿐만 아니라 결정립의 성장방향 또한 열이력의 영향을 받음을 확인할 수 있었다. 용융풀의 거동 및 형상 또한 고온균열 거동에 영향을 미침을 확인할 수 있었다. 빔 패턴을 다양하게 변화시키면서 레이저 빔 오실레이션 용접을 수행한 결과, 용융부의 조직 형성이 균열의 전파와 높은 상관관계가 있음을 증명하였다. Infinite 형상이 빔 패턴을 이용하여 용접을 수행하는 경우, 오실레이션 주파수 100 Hz, 용접속도 3.5 m/min의 조건에서 비드의 형상 뿐만 아니라 용융부를 구성하고 있는 조직, 등축정 및 주상정, 의 분포가 주기적으로 변화하는 것을 확인할 수 있었다. 이러한 현상은 레이저 빔이 패턴이 변화됨에 따라 수평방향으로 용융풀의 길이가 주기적으로 변화하며, 결과적으로 응고조직의 분포에 영향을 미침에 따라 균열 전파가 방해되었기 때문이다.

고온균열의 발생은 또한 비드의 형상과도 높은 상관관계가 존재하였다. 실험결과에서 완전용입에서 부분용입으로 용입깊이가 달라진 경우, 고온균열의 길이가 감소하였다. 비드의 형상요인과 고온균열의 길이와의 상관관계 분석을 실시하였으며, 분석결과 이면비드의 너비가 가장 높은 상관관계를 가지고 있었다. 이러한 결과를 통하여 용입깊이의 변화가 고온균열 거동에 미치는 영향을 고찰할 수 있었다.

본 연구를 통해, 아직까지 명확하게 밝혀지지 않았던 레이저 용접 중 열이력의 변화 또는 용입깊이의 변화에 따른 고온균열 거동의 이해를 증진시킬 수 있었다. 해당 연구에서는 고온균열을 제어하기 위하여 열원 프로파일 변화 및 열원모션의 변화를 제안하였으며, 이를 통해 단순 직선용접을 수행하는 경우보다 우수한 결과를 획득할 수 있음을 증명하였다. 제안된 방안이 고무적인 것은 단순히 사용된 소재뿐만 아니라 고온균열에 민감하다고 알려져 있는 여타의 소재를 대상으로도 적용이 가능하기 때문이다. 해당 연구결과를 통해 레이저의 적용가능 범위를 보다 확대시킬 수 있는 방안으로 판단된다.

핵심어: 레이저 용접, 알루미늄, 6천계열 알루미늄 합금, 자동차산업, 박판, 고온균열, 고온균열민감성, 온도구배 (G), 응고속도 (R), 조직성장, 등축정, 주상정, 결정립 크기, 결정립 성장방향, 빔 프로파일링, ARM 레이저, 레이저 빔 오실레이션, 레이저 빔 모듈레이션, 회전 주파수, 회전 너비, 레이저 빔 경로, 키홀, 용융풀 거동, 용입거동, 완전용입, 부분용입, 수치해석, 열-기계적 해석, 열전도, 잔류응력.

Student number: 2014-31061

강 민 정

감사의 글

I would like to dedicate this thesis to my loving parents and husband.
(자식을 위해 평생 헌신하신 부모님과 많은 도움을 준 신랑에게 이 논문을 바칩니다.)